Upscale Impact of Mesoscale Disturbances of Tropical Convection on Convectively Coupled Kelvin Waves

Qiu Yang* and Andrew J. Majda

Department of Mathematics and Center for Atmosphere Ocean Science, Courant Institute of Mathematical Sciences, New York University, New York, NY, USA,

Center for Prototype Climate Modeling, New York University Abu Dhabi, Saadiyat Island, Abu Dhabi, UAE

**Corresponding author address:* Qiu Yang, Courant Institute of Mathematical Sciences, New York University, 251 Mercer Street, New York, NY, 10012

E-mail: yangq@cims.nyu.edu

ABSTRACT

Tropical convection associated with convectively coupled Kelvin waves (CCKWs) is typically organized by an eastward-moving synoptic-scale convective envelope with numerous embedded westward-moving mesoscale disturbances. Such a multi-scale structure of tropical convection is a challenge for present-day cloud resolving simulations and its representation in global climate models. It is of central importance to assess upscale impact of mesoscale disturbances on CCKWs as mesoscale disturbances propagate at various tilt angles and speeds. Besides, it is still poorly understood whether the front-to-rear tilted vertical structure of CCKWs can be induced by upscale impact of mesoscale disturbances in the presence of upright mean heating. Here a simple multi-scale model is used to capture this multi-scale structure, where mesoscale fluctuations are directly driven by mesoscale heating and synoptic-scale circulation is forced by mean heating and eddy transfer of momentum and temperature. The results show that upscale impact of mesoscale disturbances that propagate at tilt angles ($110^\circ \sim 250^\circ$) induces negative lower-tropospheric potential temperature anomalies in the leading edge, providing favorable conditions for shallow convection in a moist environment, while the remaining tilt angle cases have opposite effects. Even in the presence of upright mean heating, the front-to-rear tilted synoptic-scale circulation can still be induced by eddy terms at tilt angles ($120^\circ \sim 240^\circ$). In the case with fast propagating mesoscale heating, positive potential temperature anomalies are induced in the lower troposphere, suppressing convection in a moist environment. This simple model also reproduces convective momentum transport and CCKWs in agreement with results from a recent cloud resolving simulation.

1. Introduction

Tropical rainfall is largely controlled by convectively coupled equatorial waves (CCEWs), whose dynamical and convective morphology exhibits self-similarity across multiple spatial and temporal scales (Tao and Moncrieff 2009). Among these CCEWs, CCKW is an important component of synoptic variability, which peaks along the latitude of the intertropical convergence zone (ITCZ), Africa, the Indian Ocean and South America (Kiladis et al. 2009). The early observational studies about CCKWs date back to 1970s (Wallace and Chang 1972; Zangvil 1975), when satellite-derived data on cloud brightness is utilized to define the dominant scales of motion in the tropics. The dynamical fields associated with CCKWs is characterized by low-level wind convergence leading upper-level wind divergence in a front-to-rear tilt (Yang et al. 2007a). Such horizontal and vertical structures of CCKWs are explained by stratiform instability mechanism (Mapes 2000; Majda and Shefter 2001) and also simulated by the multicloud model (MCM) (Khouider and Majda 2006c,b,a, 2008b,a; Khouider et al. 2010, 2011). Besides governing a large fraction of tropical rainfall, CCKWs are also known to interact strongly with the Madden-Julian Oscillation (MJO) (Straub et al. 2006) and link synoptic-scale variation of the Atlantic ITCZ with precipitation anomalies in South America (Wang and Fu 2007).

Instead of organizing on the synoptic scale alone, the hierarchical structure of CCKWs was identified by Nakazawa (1988) and further explained as an eastward-moving synoptic-scale convective envelope (a supercluster) with embedded westward-moving mesoscale disturbances (cloud clusters). During the 1997 Pan American Climate Studies (PACS) Tropical Eastern Pacific Process Study (TEPPS), it was observed that the large-scale convective envelope of a CCKW in the eastern Pacific ITCZ consists of many smaller-scale, westward-moving convective elements (Straub and Kiladis 2002). Similar multi-scale coherent structures of tropical convection are also observed in westward-propagating 2-day waves (Chen et al. 1996). These small-scale convective elements are categorized as mesoscale convective systems (MCSs), the dominant heavy rain producers in the tropics and subtropics (Tao and Moncrieff 2009). Squall-line systems are one particular type of MCSs and propagate at various speeds and directions (Houze 1975, 1977, 2004). In general, the multi-scale coherent structure of CCKWs with embedded mesoscale disturbances are illustrated in the conceptual diagram in Fig.1.

In spite of such progress in the observational studies, simulating multi-scale coherent structures of CCKWs with embedded mesoscale disturbances is still a challenging problem. With the development of computing resource and cloud modeling, several attempts have been done to reproduce these multi-scale features by using cloud resolving models (CRMs) in two-dimensional model setup. For example, in the trade wind regime with a strong easterly background flow, large-scale organization of tropical deep convection with numerous MCSs is investigated in idealized two-dimensional cloud resolving simulations of Grabowski and Moncrieff (2001). The convective momentum transport (CMT) from mesoscale disturbances is identified as key processes responsible for the large-scale organization of convection. In contrast, in the state of rest regime with zero mean flow, upscale transport of horizontal momentum by coherent eddy circulations is found to be small in the cloud resolving simulations of Tulich and Mapes (2008). Besides, the evidence of energy exchange through momentum transport between mesoscale disturbances and synoptic-scale propagating waves is also presented in the weather research and forecast (WRF) model (Khouider and Han 2013). There is still no clear understanding about scale interactions between synoptic-scale circulation and mesoscale disturbances. Particularly, how do mesoscale disturbances that propagate at various speeds and directions impact synoptic-scale circulation? Answering this question can not only improve our understanding about multi-scale coherent structure of tropical convection but also provide valuable intuition for convective parameterization in global climate model (GCMs).

Due to limited computing resources, it is a huge challenge for present-day GCMs in coarse resolutions to explicitly resolve those mesoscale disturbances inside large-scale organization of convection (Jiang et al. 2015). One hypothesis to explain the significant discrepancies of precipitation in GCMs is the inadequate treatment of mesoscale disturbances and their upscale impact on the large-scale organization of convection. In fact, several progresses about parameterization of organized tropical convection in GCMs have already been made. Considering the fact that countergradient vertical transport of horizontal momentum by organized convection increases wind shear and transports kinetic energy upscale, Moncrieff et al. (2017) set the archetypal dynamical models of slantwise overturning (Moncrieff 1981, 1992) into a parameterization for organized convection and its upscale effects on the resolved large-scale circulation. However, since the slantwise overturning is modeled in a two-dimensional framework, it is unclear how to parameterize the associated vertical transport of horizontal momentum if organized tropical convection has a complete three-dimensional structure and propagates at various speeds and directions. Also, the vertical structure of eddy transfer of temperature and its relative significance to impact synoptic-scale circulation is not well understood. Interestingly, the MCM (Khouider and Majda 2006c,b,a, 2008b; Khouider et al. 2010, 2011) based on three cloud types (congestus, deep and stratiform) simulates realistic features of shear-parallel MCSs in a three-dimensional structure (Khouider and Moncrieff 2015), which are commonly observed in the ITCZ. Furthermore, the stochastic multi-cloud model (SMCM) successfully captures the variability due to multi-scale organized convective systems, especially synoptic and intraseasonal variability (Goswami et al. 2017).

The goals of this paper are as follows: first, using a simple multi-scale model to capture multi-scale structures of CCKWs with embedded mesoscale disturbances and assess the associated upscale impact of mesoscale disturbances through eddy transfer of momentum and temperature; secondly, theoretically predicting the upscale impact of mesoscale disturbances propagating at various tilt angles and speeds on the mean heating driven Kelvin waves in terms of favorability for convection in a moist environment and characteristic morphology; thirdly, exploring whether the front-to-rear tilted vertical structure of CCKWs can still be induced by eddy transfer of momentum and temperature in the presence of upright mean heating; lastly, providing a useful framework to explain CMT and synoptic-scale circulation as simulated in CRMs.

The simple multi-scale model used here is the mesoscale equatorial synoptic-scale dynamics (MESD) model, originally derived by Majda (2007). The MESD model can be used to model cluster-supercluster interactions across mesoscale and synoptic scale and incorporate them together in a simple multi-scale framework. In fact, the two-dimensional version of the MESD model has already been used to model scale interactions across mesoscale and synoptic scale (Yang and Majda 2017) and concluded several crucial results as follows. It successfully reproduces many key features of synoptic-scale circulation response in a front-to-rear tilt, and compares well with results from a two-dimensional CRM (Grabowski and Moncrieff 2001). In the presence of elevated upright mean heating, the tilted vertical structure of synoptic-scale circulation can still be induced by upscale impact of mesoscale disturbances. When the large-scale convective envelope propagates faster, the upscale impact becomes less important and mean heating driven circulation response dominates. Such a result successfully explains discrepancies of numerical results in CRMs. Specifically, the simulations by Grabowski and Moncrieff (2001) in the trade wind regime with slowly propagating large-scale organization of convection feature significant CMT, while those by Tulich and Mapes (2008) in the state of rest regime with fast propagating wave packets conclude that the upscale transport of horizontal momentum by coherent eddy circulations is small. When the westward-propagating mesoscale heating has an unrealistic upward/westward tilted vertical structure, positive potential temperature anomalies are induced in the leading edge, suppressing shallow convection in a moist environment.

In this paper, several crucial results are achieved by using the three-dimensional version of the MESD model. First, explicit expressions for eddy momentum transfer (EMT) and eddy heat transfer (EHT) are obtained. The eddy transfer of horizontal momentum is along the same propagation direction as mesoscale heating. The relative strength of EHT and EMT in dimensionless units depends on the phase speed of mesoscale heating. Secondly, when mesoscale disturbances propagate at tilt angles ($110^{\circ} \sim 250^{\circ}$), negative potential temperature anomalies are induced in the leading edge, providing favorable conditions for shallow convection. Meanwhile, the upscale impact of mesoscale disturbances tends to strengthen westerlies at the surface in the mean heating driven Kelvin waves, contributing to characteristic morphology of CCKWs. When mesoscale disturbances propagate in remaining tilt angles, the upscale impact of mesoscale disturbances tend to provide unfavorable conditions for convection (positive potential temperature anomalies) and destroy coherent vertical structures of CCKWs. Thirdly, in the presence of both top-heavy and bottom-heavy upright mean heating, when the mesoscale heating propagates at tilt angles ($120^{\circ} \sim 240^{\circ}$), the front-to-rear tilted vertical structure of synoptic-scale circulation can still induced by eddy terms. Fourthly, in the case with fast propagating mesoscale heating, positive potential temperature anomalies are induced in the lower troposphere, suppressing convection in a moist environment. Lastly, by considering slowly eastward-propagating mesoscale disturbances driven by baroclinic mesoscale heating and barotropic momentum forcing, the MESD model successfully reproduces the vertical profile of CMT and CCKWs as simulated in a WRF simulation (Khouider and Han 2013).

The rest of this paper is organized as follows. Sec.2 summarizes properties of the MESD model. Sec.3 discusses the prescribed mesoscale heating propagating at a tilt angle, mesoscale fluctuations of flow field and the associated eddy transfer of horizontal momentum and temperature. Sec.4 shows the synoptic-scale circulation response to the eastward-propagating mean heating with embedded mesoscale heating propagating at a tilt angle. Sec.5 and 6 consider two different scenarios with upright mean heating and fast propagating mesoscale heating, respectively. In Sec.7, the MESD model is used to directly compare with a WRF simulation for CCKWs in terms of CMT and large-scale circulation response. The paper ends with a concluding discussion.

2. Properties of the MESD Model

In general, the multispatial-scale, multitime-scale simplified asymptotic models are derived systematically from the equatorial primitive equations, providing a useful framework to understand multi-scale phenomenon (Majda and Klein 2003; Majda 2007; Yang and Majda 2014; Majda and Yang 2016). In particular, the MESD model, originally derived by Majda (2007), describes the multitime, multispace interaction from the mesoscale to the synoptic scale, which is useful for modeling CCEWs with embedded mesoscale disturbances. Specifically, the MESD model consists of two groups of equations, one of which governs mesoscale gravity waves and the other one of which governs synoptic-scale equatorial waves including Kelvin waves, Rossby waves, mixed Rossby-gravity waves and gravity waves in the baroclinic mode as well as barotropic Rossby waves (Majda 2003).

The equations for mesoscale fluctuations in dimensionless units read as follows,

$$u_\tau = -p_x + s_u, \tag{1a}$$

$$v_\tau = -p_y + s_v, \tag{1b}$$

$$\theta_\tau + w = s_\theta, \tag{1c}$$

$$p_z = \theta, \tag{1d}$$

$$u_x + v_y + w_z = 0, \tag{1e}$$

where all physical variables stand for mesoscale fluctuations of flow fields. s_u, s_v and s_θ represent horizontal momentum forcing and diabatic heating on the mesoscale. One dimensionless unit of horizontal distance (x,y) and time τ corresponds to 150 *km* and 50 *min*, respectively.

The equations for synoptic-scale circulation in dimensionless units read as follows,

$$U_t - YV = -P_X - dU - \left\langle \overline{wu} \right\rangle_z + S_u, \tag{2a}$$

$$V_t + YU = -P_Y - dV - \left\langle \overline{wv} \right\rangle_z + S_v, \tag{2b}$$

$$\Theta_t + W = -\left\langle \overline{w\theta} \right\rangle_z + S_\theta, \tag{2c}$$

$$P_z = \Theta, \tag{2d}$$

$$U_X + V_Y + W_z = 0, \tag{2e}$$

where all capital variables stand of synoptic-scale flow fields. S_u, S_v and S_θ represent horizontal momentum forcing and diabatic heating on the synoptic scale. One dimensionless unit of horizontal distance (X,Y) and time t corresponds to 1500 *km* and 8.3 *h*, respectively. The momentum damping appearing at the right hand side of Eqs.2a and 2b is used to mimic boundary layer turbulent drag (Neelin and Zeng 2000; Majda and Shefter 2001; Biello and Majda 2006). The damping coefficient d sets the time scale of momentum dissipation, which linearly increases from 1 *day* at the surface to 10 *days* at the top. The mesoscale horizontal and temporal averaging operators are defined below for an arbitrary function f,

$$\bar{f}(X,Y) = \lim_{L\to\infty} \frac{1}{4L^2} \int_{-L}^{L} \int_{-L}^{L} f(X,x,Y,y)\, dxdy, \tag{3}$$

$$\langle f \rangle (t) = \lim_{T\to\infty} \frac{1}{2T} \int_{-T}^{T} f(t,\tau)\, d\tau, \tag{4}$$

where L is the length of the mesoscale domain and T is the time interval in the asymptotic limit. For mesoscale fluctuations of flow fields in Eqs.1a-1e, all physical variables f satisfy $\bar{f} = 0$ and $\langle f \rangle = 0$.

The MESD model is derived systematically from the primitive equations on an equatorial β-plane by following the multi-scale asymptotic procedure (Majda and Klein 2003). The derivation details can be found in Majda (2007). Eqs.1a-1e describe mesoscale fluctuations driven by some momentum and thermal forcing, while Eqs.2a-2e describe synoptic-scale circulation driven by some momentum and thermal forcing, momentum damping as well as eddy transfer of momentum and temperature. The eddy transfer of momentum and temperature, $-\langle \overline{wu} \rangle_z, -\langle \overline{wv} \rangle_z, -\langle \overline{w\theta} \rangle_z$ involve mesoscale velocity and temperature, and thus can be interpreted as upscale impact of mesoscale fluctuations on the synoptic-scale circulation. Across these two scales, several physical variables have the same dimensional value, including horizontal velocity u, v, U, V ($5\ ms^{-1}$), pressure perturbation p, P ($250\ m^2 s^{-2}$) and potential temperature anomalies θ, Θ ($3.3\ K$). However, one dimensionless unit of mesoscale vertical velocity w corresponds to $0.16\ ms^{-1}$, while that of synoptic-scale vertical velocity W is $0.016\ ms^{-1}$. Besides, both the momentum forcing and thermal forcing on the synoptic scale are assumed to be one order weaker than those on the mesoscale. Specifically, one dimensionless unit of mesoscale thermal forcing s_θ corresponds to $100\ Kday^{-1}$, while that of synoptic-scale thermal forcing S_θ is $10\ Kday^{-1}$. All physical parameters and constants are summarized in the Table.1.

a. Mesoscale gravity waves in the baroclinic modes

The governing equations for mesoscale fluctuations in Eqs.1a-1e are linear non-rotating primitive equations. In order to focus on flow fields in the free troposphere, the rigid-lid boundary conditions are imposed,

$$w = 0, \quad at\ z = 0, \pi \tag{5}$$

where $z = 0, \pi$ correspond to the surface and top of the troposphere, respectively. After plugging the ansatz for plane waves in one specific baroclinic mode,

$$f = \tilde{f} e^{i(kx+ly-\omega t)} \cos(qz), \ f \in \{u, v, p\} \tag{6}$$

$$g = \tilde{g} e^{i(kx+ly-\omega t)} \left[-q \sin(qz)\right], \ g \in \{w, \theta\} \tag{7}$$

the dispersion relation of free gravity waves reads as follows,

$$\omega \left(\omega^2 - \frac{k^2 + l^2}{q^2} \right) = 0, \tag{8}$$

where $q = 1, 2, 3...$ is vertical mode index, k, l are the wavenumber in the zonal and meridional directions and ω is the frequency. According to the Eq.8, the first mode $\omega = 0$ corresponds to the time-independent divergence-free horizontal flow, and the second and third modes $\omega = \pm\sqrt{\frac{k^2+l^2}{q^2}}$ correspond to horizontally propagating gravity waves in the baroclinic modes.

b. Mesoscale fluctuations driven by barotropic momentum forcing

By assuming all physical variables are in the barotropic mode, Eqs.1a-1e are reduced into,

$$u_\tau = -p_x + s_u, \tag{9a}$$

$$v_\tau = -p_y + s_v, \tag{9b}$$

$$u_x + v_y = 0, \tag{9c}$$

where horizontal velocity u, v and pressure p are driven by horizontal momentum forcing s_u, s_v, arising from boundary layer momentum forcing such as mountain blocking (Källén 1981). The solutions in the barotropic mode are rewritten in terms of the stream function,

$$u = -\psi_y, \tag{10}$$

$$v = \psi_x, \tag{11}$$

and further governed by,

$$(\Delta\psi)_\tau = \frac{\partial s_v}{\partial x} - \frac{\partial s_u}{\partial y}, \tag{12}$$

$$\Delta p = \frac{\partial s_u}{\partial x} + \frac{\partial s_v}{\partial y}, \tag{13}$$

which state that the time tendency of vorticity is forced by the curl of horizontal momentum forcing $\frac{\partial s_v}{\partial x} - \frac{\partial s_u}{\partial y}$, and pressure is directly determined by the divergence of horizontal momentum forcing $\frac{\partial s_u}{\partial x} + \frac{\partial s_v}{\partial y}$.

c. Synoptic-scale equatorial waves

The governing equations for synoptic-scale circulation in Eqs.2a-2e are linear primitive equations on an equatorial β-plane, forced by eddy transfer of momentum and temperature, momentum forcing and thermal forcing. Under the rigid-lid boundary conditions, the resulting equatorial waves arising from the linear primitive equations have been well studied (Matsuno 1966; Majda 2003) and also used as a methodology to isolate horizontal and vertical structures of CCEWs (Yang et al. 2007a,b,c). In spite of moist processes, these solutions share crucial features of horizontal structures and dispersion characteristics of CCEWs observed in nature (Kiladis et al. 2009).

3. Mesoscale Disturbances Propagating at a Tilt Angle

In the tropics, it is frequently observed that numerous small-scale convective elements are embedded in CCEWs such as Kelvin waves (Straub and Kiladis 2002) and 2-day waves (Haertel and Kiladis 2004). These small-scale disturbances, categorized as MCSs (Houze 2004), are typically characterized by cloud clusters and release a large amount of latent heat during tropical precipitation. In fact, the multicloud models based on three types of cloudiness (congestus, deep, stratiform) have successfully simulated multi-scale features of CCEWs in the tropics (Khouider and Majda 2006c,a, 2007, 2008a).

Squall-line systems are one particular type of MCSs and consist of a squall line forming the leading edge of the system and a trailing anvil cloud region. It has been recognized for a long time that there is a life cycle of three type clouds from congestus to deep convective to stratiform in a squall-line system. Moreover, precipitation falling from the trailing anvil cloud was stratiform and accounts for 40% of the total rain from the squall-line system (Houze 1977). Unlike eastward/westward moving equatorial waves, squall-line systems actually propagate at arbitrary tilt angles (Houze 1977) and various speeds of 5-20 ms^{-1} (Houze 1975).

In this section, the equations for mesoscale fluctuations in Eqs.1a-1e are used to model the mesoscale disturbances embedded in the synoptic-scale convective envelope. The rigid-lid boundary conditions is imposed,

$$w = 0, \text{ at} z = 0, \pi \tag{14}$$

where $z = 0, \pi$ correspond to the surface and top of the troposphere, respectively. The solutions are assumed to be periodic in the horizontal domain and have finite extent in the vertical direction.

a. Mesoscale heating propagating at a tilt angle

As mentioned above, squall-line systems could propagate at an arbitrary tilt angle. As shown by Fig.2a, here we introduce a new reference frame, one of whose axis is along the propagation direction of mesoscale heating and the other is perpendicular to that. Due to the isotropy of mesoscale dynamics in Eqs.1a-1e, it can be proved that the governing equations in this new reference are the same as those in the original reference frame. The mesoscale heating is prescribed in the first- and second-baroclinic modes as follows,

$$s_\theta = c_0 H_m\left(y'\right)\left[\sin\left(kx' - \omega\tau\right)\sin\left(z\right) + \alpha\sin\left(kx' - \omega\tau + \phi_0\right)\sin\left(2z\right)\right], \tag{15}$$

where x', y' are the horizontal coordinates in the new reference frame in Fig.2a. The constant for heating magnitude, $c_0 = 2$, corresponds to 200 $Kday^{-1}$. The zonal wavenumber $k = 2\pi$ and frequency $\omega = \frac{2\pi}{5}$ correspond to zonal wave length 150 km and period 1.73 $days$. Thus the phase speed of mesoscale heating is chosen as $c = \frac{\omega}{k} = 0.2\,(10\,ms^{-1})$. $\alpha = -\frac{2}{3}$ is the relative strength coefficient of the second-baroclinic mode, and $\phi_0 = \frac{\pi}{4}$ is the phase shift between the first- and second-baroclinic modes. The meridional profile of mesoscale heating is set to be uniform $H_m\left(y\right) = 1$, for simplicity. Fig.2b shows mesoscale heating in the new reference frame. Both heating and cooling is front-to-rear tilted, consistent with the propagation of smaller-scale disturbances in the life cycle of three type clouds as observed in reality (Houze 2004). In addition, such a top-heavy mesoscale heating is used to mimic latent heat release associated with stratiform precipitation in squall line systems (Houze 1977). Here only forced solutions with the same wavenumber k and frequency ω as the mesoscale heating in Eq.15 are discussed below.

b. Mesoscale velocity and potential temperature anomalies

Fig.3a shows vertical profiles of zonal and vertical velocity along the propagation direction. Upward motion prevails in heating regions and downward motion prevails in cooling regions. Such a deep slantwise ascending layer is considered to be crucial for maintaining a mature MCS (Moncrieff 1978, 1981; Crook and Moncrieff 1988; Moncrieff 1992). Besides, the maximum zonal and vertical velocity occurs in the upper troposphere where the maximum magnitude of mesoscale heating is reached. In addition, at the lower troposphere, wind divergence (convergence) is located in the mesoscale cooling (heating) regions, while such a relation is reversed in the upper troposphere.

Fig.3b shows vertical profile of potential temperature anomalies along the propagation direction. Similarly, potential temperature anomalies also have a front-to-rear tilt. Besides, the vertical structure of potential temperature anomalies are significantly dominated by the second-baroclinic mode. In heating regions such as the longitude $1.9 \times 10^2 km$, positive anomalies are sitting on top of negative anomalies, resembling the observation that in a MCS, latent heat is released on top due to stratiform precipitation and cooling effects are induced below due to rain evaporation (Houze 2004).

c. Eddy momentum transfer and eddy heat transfer

The eddy zonal momentum transfer (EZMT) in Eq.2a is formulated by vertical gradient of eddy fluxes of zonal momentum in a negative sign and reads in dimensionless units as follows,

$$\begin{aligned} F^u &= -\left\langle \overline{w'u'} \right\rangle_z \\ &= \cos(\gamma)\, \kappa^u \left[-\frac{3}{2}\cos(z) + \frac{3}{2}\cos(3z) \right], \end{aligned} \tag{16}$$

where γ is the tilt angle of mesoscale heating. The coefficient κ^u has the following explicit expression,

$$\kappa^u = \frac{c_0^2 \sin(\phi_0)\,\alpha k^3}{2(\omega^2 - k^2)(4\omega^2 - k^2)}, \tag{17}$$

which directly determines the strength and direction of EZMT. First, the coefficient κ^u is proportional to the product term $\sin(\phi_0)\,\alpha$, indicating that one necessary condition for nonvanishing EZMT is nonzero phase shift ϕ_0 and relative strength α. Secondly, the product term $k^3 \sin(\phi_0)\,\alpha$ determines the sign of the numerator of Eq.17, controlling the direction of EZMT. Lastly, the expression in Eq.17 has two critical absolute phase speeds $c = \frac{\omega}{k} = \pm 1, \pm\frac{1}{2}$, the same as the phase speeds of gravity waves in the first- and second-baroclinic modes as shown in Eq.8.

The eddy meridional momentum transfer (EMMT) in Eq.2b is formulated by vertical gradient of eddy fluxes of meridional momentum in a negative sign and reads in dimensionless units as follows,

$$\begin{aligned} F^v &= -\left\langle \overline{w'v'} \right\rangle_z \\ &= \sin(\gamma)\,\kappa^u \left[-\frac{3}{2}\cos(z) + \frac{3}{2}\cos(3z) \right], \end{aligned} \tag{18}$$

whose coefficient κ^u is exactly the same as Eq.17. In fact, EZMT in Eq.16 and EMMT in Eq.18 can be rewritten into a vector form,

$$\begin{pmatrix} F^u \\ F^v \end{pmatrix} = \kappa^u \left[-\frac{3}{2}\cos(z) + \frac{3}{2}\cos(3z) \right] \begin{pmatrix} \cos(\gamma) \\ \sin(\gamma) \end{pmatrix}, \tag{19}$$

which states that the eddy transfer of horizontal momentum is actually along the same direction of mesoscale heating, directing at the tilt angle γ.

The EHT in Eq.2c is formulated by vertical gradient of eddy fluxes of temperature in a negative sign and reads in dimensionless units as follows,

$$\begin{aligned} F^{\theta} &= -\left\langle \overline{w'\theta'} \right\rangle_z \\ &= \kappa^{\theta} \left[\frac{3}{2} \sin(z) - \frac{9}{2} \sin(3z) \right], \end{aligned} \tag{20}$$

whose coefficient,

$$\kappa^{\theta} = \frac{c_0^2 \sin(\phi_0) \, \alpha k^3 c}{2 \left(\omega^2 - k^2\right) \left(4\omega^2 - k^2\right)}, \tag{21}$$

directly determines the strength and sign of EHT. The ratio between κ^{θ} and κ^{u} in dimensionless units is equal to

$$\frac{\kappa^{\theta}}{\kappa^{u}} = c, \tag{22}$$

which is proportional to the phase speed $c = \frac{\omega}{k}$ of the mesoscale heating in Eq.15. Since EZMT, EMMT and EHT further drive synoptic-scale circulation in Eqs.2a-2e, Eq.22 states that the phase speed of mesoscale heating determines the relative strength of synoptic-scale circulation response to these eddy terms.

Fig.4a shows the vertical profile of eddy zonal momentum flux $\overline{w'u'}$, which reaches its minimum value at the middle troposphere $z = 7.85km$ and decays to zero as the height goes close to the surface and top. Correspondingly, EZMT reaches its minimum value at $11km$ and maximum value at $z = 5km$. As shown by Eq.16, the first- and third-baroclinic modes in EZMT have equal strength but opposite signs, thus EZMT vanishes at the surface and top. In fact, such a spatial pattern of zonal momentum flux has already been investigated in an idealized two-dimensional cloud-resolving simulations (Grabowski and Moncrieff 2001).

Fig.4b shows the vertical profile of eddy potential temperature flux $\overline{w'\theta'}$, which reaches the maximum value at $11km$ and the minimum value at $5km$ and decays as the height goes close to the top, the middle and the surface. Correspondingly, EHT reaches its maximum value at $13km$

and $3km$ but the minimum value at $7.85km$. In a moist environment, such a heating in the lower troposphere below the height $5km$ tends to suppress the convection by increasing saturation rate of vapor and convective inhibition (CIN).

4. Convectively Coupled Kelvin Waves with Embedded Mesoscale Disturbances

As discussed in Sec.3, mesoscale disturbances of tropical convection in a front-to-rear tilt tend to generate eddy transfer of horizontal momentum and temperature, further driving the synoptic-scale circulation. In this section, the synoptic-scale circulation response to both upscale impact of mesoscale fluctuations and mean heating is discussed, in terms of low-tropospheric potential temperature anomalies and horizontal velocity and temperature at various levels.

Here the equations for synoptic-scale circulation in Eqs.2a-2e are used. As for boundary conditions, the solutions are assumed to be periodic in the zonal direction and decay as the latitude increases. In the vertical direction, the rigid-lid boundary condition is imposed,

$$W = 0, \text{at}\, z = 0, \pi \tag{23}$$

where $z = 0, \pi$ denote the surface and top of the troposphere, respectively. The actual numerical simulations are implemented in the domain (longitude, latitude, height), $0 \leq x < 3 \times 10^4 km$, $-2 \times 10^3 km < y < 2 \times 10^3 km$, $0 \leq z \leq 15.7km$. All physical variables are initialized from the background state of rest and plotted at day 13.8.

a. Synoptic-scale mean heating and mesoscale heating modulated by a large-scale envelope

The synoptic-scale mean heating is prescribed in the following general expression,

$$S_\theta = F(X - st, z)\, H(Y), \tag{24}$$

where $F(X-st,z)$ denotes the zonal/vertical profile of mean heating at the propagating speed $s = 15ms^{-1}$. The meridional profile $H(Y)$ is chosen as the first parabolic cylinder function (Majda 2003) for simplicity,

$$H(Y) = \pi^{-\frac{1}{4}} e^{-\frac{Y^2}{2}}, \tag{25}$$

which reaches its maximum value at the equator and decays as the latitude increases. Fig.5a shows the vertical profile of tilted mean heating in the longitude-height diagram. This tilted mean heating consists of a strong heating region in the middle with a strong (weak) cooling region to the west (east), all of which are characterized by a front-to-rear tilt. Such a front-to-rear tilt of organized tropical convection is typically observed across multiple scales (Houze 2004; Kiladis et al. 2009). Fig.5b-c show vertical profiles of the top-heavy and bottom-heavy upright mean heating, which will be used in Sec.5.

The modulation of mesoscale disturbances in a convective envelope is represented by a synoptic-scale envelope function in the following form,

$$E(X-st,Y) = \begin{cases} \cos\left(\frac{\pi(X-st)}{2L}\right) H(Y) & -L \leq X \leq L \\ 0 & \text{otherwise} \end{cases}, \tag{26}$$

where the propagating speed of the envelope, $s = 15ms^{-1}$, is picked the same as Eq.24, the typical phase speed of CCKWs observed in the eastern Pacific (Straub and Kiladis 2002) and the Indian Ocean (Kiladis et al. 2009). $L = 2$ (3000 km) is half extent of the convective envelope. Therefore, the mesoscale heating modulated by a convective envelope is prescribed as follows,

$$s_\theta = E(X-st,Y)\, c_0 H_m(y') \left[\sin\left(kx' + \omega\tau\right)\sin(z) + \alpha \sin\left(kx' + \omega\tau + \phi_0\right)\sin(2z)\right], \tag{27}$$

where all physical parameters and constants are the same as Eq.15, except that the frequency ω is reduced to $\frac{\pi}{5}$ (phase speed $c = \frac{\omega}{k}$ is reduced to 5 ms^{-1}).

b. Potential temperature anomalies in the lower troposphere

In a moist environment, negative potential temperature anomalies in the lower troposphere provide favorable conditions for convection through decreasing saturation rate of vapor, CIN, and increasing convective available potential energy (CAPE). As a counterpart of that, positive anomalies provide unfavorable conditions for convection. Here lower-tropospheric potential temperature anomalies induced by mean heating and eddy terms (EZMT,EMMT, EHT) at various tilt angles are discussed. The goal here is to understand upscale impact of mesoscale disturbances that propagate at various tilt angles on lower-tropospheric potential temperature and interpret the associated favorability for convection in a moist environment. Considering the fact that flow fields will just be mirror-symmetric if the tilt angle is reflected about the equator, the cases at tilt angles, $0 \leq \gamma \leq \pi$, are only considered here.

Fig.6a show the horizontal profile of lower-tropospheric potential temperature anomalies induced by mean heating at 2.62 km, which is characterized by warm anomalies in the middle and cold anomalies to the east and west. Fig.6b-h show horizontal profiles of lower-tropospheric potential temperature anomalies induced by eddy terms. As summarized by Fig.6i, the upscale impact of mesoscale disturbances that propagate at various tilt angles are divided into three categories. In the blue region ($110^\circ \sim 250^\circ$) such as Fig.6b-c, eddy terms induce negative lower-tropospheric potential temperature anomalies in the leading edge of the convective envelope. In a moist environment, such lower-tropospheric negative anomalies provide favorable conditions for convection, initializing new shallow convection in the leading edge and preconditioning deep convection as the whole convective envelope propagates eastward. In the pink region ($70^\circ \sim 110^\circ$ and $250^\circ \sim 290^\circ$) such as Fig.6d-f, eddy terms induce positive lower-tropospheric potential temperature anomalies off the equator in the leading edge, providing unfavorable conditions for shallow convection and resulting in an asymmetric meridional profile of the convective envelope. In the red region ($0^\circ \sim 70^\circ$ and $290^\circ \sim 360^\circ$) such as Fig.6g-h, eddy terms induce positive lower-tropospheric potential temperature anomalies in the leading edge. In a moist environment, such strong positive anomalies provide unfavorable conditions for convection, suppressing shallow convection and further destroying coherent structures of CCKWs. This result explains the fact that most of mesoscale disturbances in CCKWs propagate westward in nature (Nakazawa 1988; Straub and Kiladis 2002), instead of eastward.

c. Horizontal velocity and pressure perturbation at different levels

Here horizontal velocity and pressure perturbation induced by mean heating and eddy terms at various tilt angles are discussed and interpreted in terms of their impact on characteristic morphology of CCKWs, favorability for tropical cyclogenesis, and moisture transport in a moist environment. The goal is to understand how upscale impact of mesoscale disturbances that propagate at different tilt angles modifies the mean heating driven circulation.

Fig.7a shows the horizontal profile of mean heating driven horizontal velocity and pressure perturbation at the surface, which are characterized by zonal wind convergence and an east-west dipole of pressure perturbation. By comparing the flow fields induced by eddy terms with the mean heating driven circulation, several crucial results are obtained. In the cases with tilt angles (180°, 135°) in Figs.7b-c, the westerlies induced by eddy terms tend to strengthen (weaken) the westerlies (easterlies) from the mean heating driven circulation, pushing the longitude of wind convergence to further east. Such strengthened westerlies in the convection region led by wind convergence to the east resemble the typical wind field associated with CCKWs at the surface (Yang et al. 2007a). Meanwhile, eddy terms induce negative pressure perturbation in the leading edge, resulting in convergence of winds and moisture and providing favorable conditions for tropical cyclogenesis.

In the cases with tilt angles (110°, 90°, 70°) in Fig.7d-f, northeasterly winds are induced by eddy terms in the Northern Hemisphere, introducing meridional asymmetry of mean heating driven circulation with strengthened easterlies off the equator. In the cases with tilt angles (45°, 0°) in Fig.7g-h, significant easterlies induced by eddy terms tend to weaken (strengthen) the westerlies (easterlies) from the mean heating driven circulation. Also, positive pressure perturbation induced by eddy terms provides unfavorable conditions for tropical cyclogenesis.

Fig.8 shows horizontal profiles of horizontal velocity and pressure perturbation at the lower troposphere. In the cases with tilt angles (180°, 135°) in Fig.8b-c, the lower-tropospheric easterlies induced by eddy terms tend to strengthen the inflow of mean heating driven circulation in the leading edge, bringing moisture into the convective envelope and preconditioning deep convection in a moist environment. In the cases with tilt angles (110°, 90°, 70°) in Fig.8d-f, eddy terms induce significant westerlies in the Northern Hemisphere with positive pressure perturbation, resulting in meridional asymmetry of dynamical fields. In the cases with tilt angles (45°, 0°) in Fig.8g-h, the strong westerlies and positive pressure perturbation induced by eddy terms tend to destroy the mean heating driven circulation.

Fig.9 shows horizontal profiles of horizontal velocity and pressure perturbation at the upper troposphere. In particular, the flow fields induced by eddy terms at tilt angles (180°, 135°) in Fig.9b-c are characterized by significant westerlies winds in the upper troposphere, which tend to strengthen the outflow in the leading edge, result in strong vertical shear of zonal winds between the lower and upper tropospheres and provide favorable conditions for convection (Moncrieff 1978). Fig.10 shows horizontal profiles of horizontal velocity and pressure perturbation at the top. In particular, in the cases with tilt angles (180°, 135°) in Fig.10b-c, easterlies and negative pressure perturbation induced by eddy terms tend to strengthen the easterly winds in the mean heating driven circulation in the trailing edge but weaken the westerlies winds in the leading edge.

5. Upright mean heating

The goal of this section is to explore whether the upward/westward tilted vertical structure of zonal velocity, potential temperature anomalies can still be induced by eddy terms, in the presence of upright mean heating. Specifically, both top-heavy and bottom-heavy upright mean heating shown in Fig.5b-c are considered. All model setup is exactly the same as Sec.4. It turns out that the relative location between the mean heating and convective envelope for mesoscale heating plays an important role here and thus it is carefully chosen below.

a. Top-heavy upright mean heating

Fig.11a shows the vertical profile of potential temperature anomalies induced by top-heavy upright mean heating. Although the upright mean heating has only significant anomalies in the upper troposphere, the resulting potential temperature anomalies feature significant second-baroclinic mode to the east and cold upper-tropospheric anomalies to the west. Fig.11c-f show vertical profiles of potential temperature anomalies induced by eddy terms at various tilt angles. The resulting anomalies are dominated by significant third-baroclinic mode, whose signs change as the tilt angle switches from westward to eastward. Fig.11g-j show vertical profiles of total potential temperature anomalies induced by mean heating and eddy terms. As summarized in Fig.11b, all these cases at various tilt angles are divided into two categories. In the blue region ($120^\circ \sim 240^\circ$) such as Fig.11g-h, the tilted vertical structure of potential temperature anomalies can still be induced by eddy terms, in the presence of top-heavy upright mean heating. The corresponding total zonal velocity in Fig.12f-g resembles the zonal winds in large-scale organization of convection as simulated in the cloud resolving model (Grabowski and Moncrieff 2001). In the red region ($0^\circ \sim 120^\circ$ and $240^\circ \sim 360^\circ$) such as Fig.11i-j and Fig.12h-i, no tilted vertical structure of potential temperature anomalies and zonal velocity are induced by eddy terms, in the presence of top-heavy upright mean heating. The upper-tropospheric zonal velocity induced by eddy terms in Fig.12d-e tends to strengthen upper-tropospheric easterlies and westerlies in the leading edge from the mean heating driven circulation.

b. Bottom-heavy upright mean heating

Fig.13a shows the vertical profile of potential temperature anomalies induced by bottom-heavy mean heating. The resulting potential temperature anomalies share the similar spatial pattern as Fig.11a but in the opposite sign. As summarized in Fig.13b and Fig.14b, all these cases at various tilt angles are divided into two categories. In the blue region ($120^\circ \sim 240^\circ$) such as Fig.13g-h and Fig.14g-h,the tilted vertical structure of zonal velocity and potential temperature anomalies can still be induced by eddy terms in the presence of bottom-heavy upright mean heating. Specifically, Fig.13g-h shows tilted positive potential temperature anomalies with its maximum value in the lower troposphere, while Fig.14g-h shows an upward/westward inflow layer with easterlies. Easterly winds are also noted near the top. Fig.14g-h. However, in the red region ($0^\circ \sim 120^\circ$ and $240^\circ \sim 360^\circ$) such as Fig.13i-j and Fig.14i-j, no tilted vertical structure of zonal velocity and potential temperature anomalies are induced by eddy terms.

6. Faster Propagating Mesoscale Heating

The early observation about MCSs such as tropical squall lines dates back to 1970s. For example, during phase III of GATE, four squall lines passed over the U.S. NOAA ship Researcher (Houze 1975). According to Houze (1975), propagating speeds of squall line systems vary from $5ms^{-1}$ to $20ms^{-1}$. In Sec.4, the propagation speed of mesoscale heating is set as $5ms^{-1}$. According to Eq.22, such a slow propagation speed of mesoscale heating means that the synoptic-scale circulation response to EMT is much stronger than that to EHT. In this section, a faster propagating mesoscale heating ($15ms^{-1}$) is considered so that the synoptic-scale circulation response to EHT dominates. The goal is to understand the upscale impact of fast propagating mesoscale disturbances on synoptic-scale potential temperature anomalies.

Fig.15a shows the vertical profile of potential temperature anomalies induced by mean heating. Similar to mean heating, the resulting potential temperature anomalies are also characterized by a front-to-rear tilt. As shown in Fig.15b, potential temperature anomalies induced by EHT are dominated by the third-baroclinic mode with cold anomalies in the middle troposphere and warm anomalies in both upper and lower tropospheres. Potential temperature anomalies induced by EZMT at the tilt angle 180° and 0° are manifested by the third-baroclinic mode but in the opposite signs in Fig.15c-d. Fig.15e-f shows total potential temperature anomalies induced by eddy terms at the tilt angle 180° and 0°. In these two cases, the anomalies are both characterized by warm anomalies in the lower troposphere, providing unfavorable conditions for shallow convection in a moist environment. Specifically, potential temperature anomalies induced by EHT in Fig.15b compete with those induced by EZMT in Fig.15c. Thus in the case with westward-propagating mesoscale heating in Fig.15e, the total anomalies induced by eddy terms have weak magnitude in the trailing edge. In contrast, potential temperature anomalies induced by EHT in Fig.15b and those induced by EZMT in Fig.15d strengthen each other. Thus in the case with eastward-propagating mesoscale heating in Fig.15f, the total potential temperature anomalies induced by eddy terms have strong magnitude and are mostly located in the leading edge. Lastly, according to Fig.15e, the maximum magnitude of potential temperature anomalies induced by EHT and EZMT increases as mesoscale heating propagates faster, while their relative strength decreases, consistent to the result in Eq.22. The threshold propagating speed when they have equal strength is around $12\ ms^{-1}$.

7. Comparison with a WRF Simulation for Convectively Coupled Kelvin Waves

In Khouider and Han (2013), idealized simulations of CCKWs are implemented in the WRF model, which reproduces a coherent eastward propagating CCKW with many common features as observed in nature. Furthermore, the evidence of energy exchange, through momentum transport, between small-scale circulation due to mesoscale convection and the propagating synoptic scale waves is also included. In this section, the MESD model is set in the same model setup as that in Khouider and Han (2013). The goals are to explain the vertical profile of CMT and reproduce the total synoptic-scale circulation as simulated in Khouider and Han (2013), including zonal velocity and potential temperature anomalies.

a. Barotropic momentum forcing and baroclinic heating on the mesoscale

Mesoscale heating thermally drives mesoscale fluctuations of velocity, pressure perturbation and potential temperature anomalies in the free tropical atmosphere. In reality, mesoscale fluctuations can also be impacted by momentum forcing through the boundary layer dynamics such as the orographic effects (McFarlane 1987) and sea surface temperature gradient (Lindzen and Nigam 1987; Wang and Li 1993). For example, the barotropic mode of the boundary layer dynamics was considered in a multi-scale model for the Madden-Julian Oscillation (Biello and Majda 2006).

Here we first generalize mesoscale heating with a localized meridional profile in a full three-dimensional structure,

$$s_\theta = c_0\left[1+\sin\left(ly'\right)\right]\left[\sin\left(kx'-\omega\tau\right)\sin\left(z\right)+\alpha\sin\left(kx'-\omega\tau+\phi_0\right)\sin\left(2z\right)\right], \qquad (28)$$

where x', y' represent the zonal and meridional coordinates in the new reference frame at a tilt angle γ. All physical parameters and constant are the same as Eq.15. Besides, a zonal momentum forcing in the barotropic mode is also prescribed,

$$s_u = c_1 \left[1+\sin\left(ly'\right)\right] \sin\left(kx' - \omega\tau + \phi_b\right), \tag{29}$$

where $c_1 = -0.52$ denotes the magnitude of barotropic momentum forcing. The parameter $\phi_b \in [-\pi, \pi)$ represents the phase shift between the mesoscale heating in the first baroclinic mode in Eq.28 and the zonal momentum forcing in the barotropic mode in Eq.29. Here ϕ_b is picked to be the same as $\phi_0 = \frac{\pi}{2}$. Positive (negative) phase shift ϕ_b means that zonal momentum forcing s_u lags (leads) mesoscale heating s_θ.

Fig.16a shows the vertical profile of zonal velocity induced by mesoscale heating. The resulting zonal velocity is characterized by a front-to-rear tilt. In contrast, the zonal velocity induced by the barotropic momentum forcing is upright with an alternate zonal profile in Fig.16b. As shown in Fig.16c, the total zonal velocity still has a significant upward/westward tilted vertical structure, resembling the typical zonal winds associated with MCSs. Meanwhile, the total vertical velocity also has a front-to-rear tilt in an alternate zonal profile in Fig.16c.

b. Eddy momentum transfer and eddy heat transfer

In Sec.3, the EMT and EHT driven by the tilted mesoscale heating consist of the first- and third-baroclinic modes. In the presence of the barotropic mode, the interaction between the barotropic mode and baroclinic modes generate extra first- and second-baroclinic modes in EMT. The full expressions of EMT and EHT in dimensionless units read as follows,

$$\begin{aligned} F^u &= -\left\langle \overline{w'u'} \right\rangle_z \\ &= \cos(\gamma)\left[\left(\kappa_1^u - \frac{3}{2}\kappa^u\right)\cos(z) + \kappa_2^u\cos(2z) + \frac{3}{2}\kappa^u\cos(3z)\right], \end{aligned} \tag{30}$$

$$F^v = -\left\langle \overline{w'v'} \right\rangle_z$$
$$= \sin(\gamma)\left[\left(\kappa_1^u - \frac{3}{2}\kappa^u\right)\cos(z) + \kappa_2^u \cos(2z) + \frac{3}{2}\kappa^u \cos(3z)\right], \tag{31}$$

$$F^\theta = -\left\langle \overline{w'\theta'} \right\rangle_z$$
$$= \kappa^\theta \left[\frac{3}{2}\sin(z) - \frac{9}{2}\sin(3z)\right], \tag{32}$$

where γ is the tilt angle and coefficients $\kappa_1^u, \kappa_2^u, \kappa^u, \kappa^\theta$ are listed in the Appendix.

Fig.17a shows the vertical profile of EZMT, which is characterized by the third baroclinic mode with alternate value at different levels. Such a vertical profile of EZMT resembles that from the WRF simulation of Khouider and Han (2013) in Fig.17b, where positive value of CMT is found at the lower troposphere and top and negative value of CMT is found at the surface and the upper troposphere. The EHT in Fig.17c has much weaker magnitude but the same profile as Fig.4b.

c. Zonal velocity and potential temperature anomalies on the synoptic scale

In this section, the synoptic-scale circulation response to EMT and EHT from the MESD model, including zonal velocity and potential temperature, is directly compared with those as simulated in Khouider and Han (2013). Two central questions are addressed here, that is, whether the total circulation response induced by mean heating and eddy terms resembles those from Khouider and Han (2013) and what is the upscale impact of CMT on the synoptic-scale circulation.

Fig.18 shows vertical profiles of total zonal velocity induced by mean heating and eddy terms at the equator. As shown in Fig.18a, the mean heating driven zonal velocity has a front-to-rear tilt with zonal wind convergence (divergence) at the surface (top) in heating regions. In contrast, the zonal velocity induced by eddy terms in Fig.18b features significant third-baroclinic mode with its maximum value at the top. When compared with mean heating driven zonal velocity in Fig.18a, the zonal velocity induced by eddy terms tends to strengthen mean heating driven westerlies at the top, lift up the easterlies at the middle troposphere and weaken the westerlies at the surface. As shown by Fig.18c, the total zonal velocity resembles many features of zonal velocity from the WRF simulation in Fig.18d, such as the strong westerlies at the level 250hPa and the easterlies at the level 400hPa.

Fig.19 shows vertical profiles of potential temperature anomalies induced by mean heating and eddy terms at the equator. The mean heating driven potential temperature anomalies are upward/westward tilted in Fig.19a. The anomalies induced by eddy terms feature a significant third-baroclinic mode in Fig.19b. It turns out that the anomalies induced by eddy terms tend to weaken mean heating driven negative anomalies at lower troposphere and positive anomalies in the middle troposphere but add extra positive anomalies in the upper troposphere. The resulting total potential temperature anomalies share several common features as those from the WRF simulation in Fig.19d, such as the two positive maximum anomalies at both lower and upper troposphere and negative anomalies in the trailing edge.

8. Concluding Discussion

The goals of this paper include the following four aspects: first, using a simple multi-scale model to capture multi-scale structures of CCKWs with embedded mesoscale disturbances and assess upscale impact of mesoscale disturbances through eddy transfer of momentum and temperature; secondly, theoretically predicting the upscale impact of mesoscale disturbances that propagate at various tilt angles and speeds on the mean heating driven Kelvin waves in terms of favorability for convection in a moist environment and characteristic morphology; thirdly, exploring whether the front-to-rear tilted vertical structure of CCKWs can still be induced by eddy transfer of momentum and temperature in the presence of upright mean heating; lastly, providing a useful framework to explain CMT and synoptic-scale circulation as simulated in CRMs.

The simple multi-scale model used here is the MESD model, originally derived by Majda (2007). It consists of two groups of equations on mesoscale and synoptic scale, respectively. Specifically, mesoscale fluctuations of flow field are directly driven by a prescribed mesoscale heating in a front-to-rear tilt in the first- and second-baroclinic modes. The resulting EMT and EHT are expressed in an explicit form and further interpreted as the upscale impact of mesoscale fluctuations on the synoptic-scale circulation. Such explicit expressions for eddy transfer of momentum and temperature should be useful to improve parameterization of upscale impact of mesoscale tropical convection in the GCMs. In connection with the minimalist second baroclinic convective momentum transport as implemented in Moncrieff et al. (2017), the EMT from the MESD model shares similar vertical profile in the interior but has vanishing value at the surface and top. Meanwhile, the MESD model shows that eddy transfer of horizontal momentum is along the same direction as the propagation direction of mesoscale heating, providing a simple way to generalize CMT parameterization for both zonal and meridional momentum. The direction of EMT is determined by the tilt angle of mesoscale heating, which may further depend on the large-scale background flow or wind shear. Also, the EHT dominated by the third-baroclinic mode could be another important component in the parameterization of organized tropical convection in the GCMs. The MESD model shows that the relative strength of EHT and EMT in dimensionless units depends on the propagating speed of mesoscale heating, highlighting the dominant magnitude of EMT in the slowly propagating mesoscale heating cases.

By focusing on low-tropospheric potential temperature anomalies, the MESD model theoretically predicts that the upscale impact of mesoscale disturbances favors shallow convection in the leading edge at tilt angles ($110^{\circ} \sim 250^{\circ}$), while it suppresses shallow convection at tilt angles (less than 70° or larger than 290°). Such a result explains the observation that most of mesoscale disturbances propagate westward in CCKWs and few of them propagate eastward (Straub and Kiladis 2002). In the remaining tilt angles, the MESD model shows that the upscale impact of mesoscale disturbances provides unfavorable conditions for shallow convection off the equator, explaining the meridional asymmetry of convection as CCKWs propagate eastward along the equator. In the tilt angles ($135^\circ \sim 180^\circ$), the upscale impact of mesoscale disturbances is found to strengthen the westerlies at the surface, the inflow at the lower troposphere and the outflow at the upper troposphere. However, it tends to destroy coherent structures of CCKWs in the remaining tilt angle cases.

It is frequently observed that vertical structures of tropical convection is characterized by a front-to-rear tilt, which shows self-similarity across multiple spatial and temporal scales (Houze 2004; Kiladis et al. 2009). It is important to understand how much of tilted vertical structures of tropical convection is induced by upscale impact of mesoscale fluctuations, instead of mean heating. The MESD model shows that the synoptic-scale circulation in a front-to-rear tilt can still be induced by eddy terms at tilt angles ($120^\circ \sim 240^\circ$) in the presence of upright mean heating, indicating the significant contribution of upscale impact of mesoscale disturbances on characteristic morphology of CCKWs.

In the case with fast propagating mesoscale heating, the MESD model shows that the synoptic-scale circulation response to EHT dominates and induces positive potential temperature anomalies in the lower troposphere, providing unfavorable conditions for shallow convection in a moist environment. Such a result explains the observation that most of mesoscale disturbances inside the convective envelope of CCKWs propagate slowly in reality.

In order to compare with results from the WRF simulation by Khouider and Han (2013), slowly eastward-propagating mesoscale disturbances driven by baroclinic mesoscale heating and barotropic momentum forcing are considered along with the front-to-rear tilted mean heating. The MESD model successfully reproduces the vertical profile of CMT in the third-baroclinic mode and the total synoptic-scale circulation, providing encouraging evidence for validating this simple multi-scale model. Nevertheless, such a theoretical explanation about the results from a WRF simulation requires more validation by cloud resolving simulations in various model setup. One essential motivation of this paper is to inspire more detailed examination on the spatial pattern of mesoscale disturbances and the associated CMT in WRF simulations for CCKWs.

The MESD model could also be used to model many other multi-scale phenomenon such as westward-propagating 2-day waves (Haertel and Kiladis 2004) and easterly waves in the ITCZ (Toma and Webster 2010a,b). Meanwhile, it can be elaborated and generalized in various ways. The first interesting research direction is to couple boundary layer dynamics with that in the free troposphere, in a similar way as Biello and Majda (2006). The augmented model should be useful to capture more realistic features of CCEWs in the equatorial regions such as the ITCZ. The second research direction is to introduce a two-way feedback between the synoptic-scale circulation and mesoscale heating. For instance, the tilt angle in which direction mesoscale heating propagates could also be influenced by large-scale winds. Such a two-way feedback may come up with an instability mechanism for CCEWs in the tropics. The third research direction is to couple the MESD model with an active heating function such as the MCM (Khouider and Majda 2006c,b,a, 2008b,a; Khouider et al. 2010, 2011). The resulting model allows two-way feedbacks between circulation and heating, providing a simple testbed to study convective instability.

Acknowledgments. This research of A.J.M is partially supported by the office of NAVAL Research ONR MURI N00014-12-1-0912, and Q.Y. is supported as a graduate research assistant on this grant and partially funded as a postdoctoral fellow by the Center for Prototype Climate Modelling (CPCM) in New York University Abu Dhabi (NYUAD) Research Institute.

APPENDIX

Coefficients of Eddy Momentum Transfer and Eddy Heat Transfer

Here coefficients of EMT and EHT in Eqs.30-32 is explicitly listed in the following expressions,

$$\kappa_1^u = -\frac{c_0 c_1 l^2 \sin(\phi_b)}{4\omega(\omega^2 - k^2 - l^2)}, \tag{A1}$$

$$\kappa_2^u = -\frac{c_0 c_1 \alpha l^2 \sin(\phi_b - \phi_0)}{2\omega(4\omega^2 - k^2 - l^2)}, \tag{A2}$$

$$\kappa^u = \frac{c_0^2 \alpha \sin(\phi_0) k}{2}\left[\frac{k^2}{(\omega^2 - k^2)(4\omega^2 - k^2)} + \frac{(k^2 + l^2)}{2(\omega^2 - k^2 - l^2)(4\omega^2 - k^2 - l^2)}\right], \tag{A3}$$

$$\kappa^\theta = \frac{c_0^2 \alpha \sin(\phi_0)\omega}{2}\left[\frac{k^2}{(\omega^2 - k^2)(4\omega^2 - k^2)} + \frac{(k^2 + l^2)}{2(\omega^2 - k^2 - l^2)(4\omega^2 - k^2 - l^2)}\right], \tag{A4}$$

where all physical parameters and constants are the same as Eqs.28-29.

References

Biello, J. A., and A. J. Majda, 2006: Modulating synoptic scale convective activity and boundary layer dissipation in the IPESD models of the Madden–Julian oscillation. *Dynamics of atmospheres and oceans*, **42 (1)**, 152–215.

Chen, S. S., R. A. Houze, Jr., and B. E. Mapes, 1996: Multiscale variability of deep convection in realation to large-scale circulation in TOGA COARE. *Journal of the Atmospheric Sciences*, **53 (10)**, 1380–1409.

Crook, N. A., and M. W. Moncrieff, 1988: The effect of large-scale convergence on the generation and maintenance of deep moist convection. *Journal of the atmospheric sciences*, **45 (23)**, 3606–3624.

Goswami, B., B. Khouider, R. Phani, P. Mukhopadhyay, and A. J. Majda, 2017: Improving synoptic and intra-seasonal variability in CFSv2 via stochastic representation of organized convection. *Geophysical Research Letters*, **44 (2)**, 1104–1113.

Grabowski, W. W., and M. W. Moncrieff, 2001: Large-scale organization of tropical convection in two-dimensional explicit numerical simulations. *Quarterly Journal of the Royal Meteorological Society*, **127 (572)**, 445–468.

Haertel, P. T., and G. N. Kiladis, 2004: Dynamics of 2-day equatorial waves. *Journal of the Atmospheric Sciences*, **61 (22)**, 2707–2721.

Houze, R. A., Jr., 1975: Squall lines observed in the vicinity of the researcher during phase III of GATE. *Preprints, 16th Radar Meteorology Conf., Houston, TX, American Meteorological Society*, 206–209.

Houze, R. A., Jr., 1977: Structure and dynamics of a tropical squall-line system. *Monthly Weather Review*, **105 (12)**, 1540–1567.

Houze, R. A., Jr., 2004: Mesoscale convective systems. *Reviews of Geophysics*, **42 (4)**.

Jiang, X., and Coauthors, 2015: Vertical structure and physical processes of the Madden-Julian oscillation: Exploring key model physics in climate simulations. *Journal of Geophysical Research: Atmospheres*, **120 (10)**, 4718–4748.

Källén, E., 1981: The nonlinear effects of orographic and momentum forcing in a low-order, barotropic model. *Journal of the Atmospheric Sciences*, **38 (10)**, 2150–2163.

Khouider, B., J. Biello, and A. J. Majda, 2010: A stochastic multicloud model for tropical convection. *Communications in Mathematical Sciences*, **8 (1)**, 187–216.

Khouider, B., and Y. Han, 2013: Simulation of convectively coupled waves using WRF: a framework for assessing the effects of mesoscales on synoptic scales. *Theoretical and Computational Fluid Dynamics*, **27 (3-4)**, 473–489.

Khouider, B., and A. J. Majda, 2006a: Model multi-cloud parameterizations for convectively coupled waves: Detailed nonlinear wave evolution. *Dynamics of atmospheres and oceans*, **42 (1)**, 59–80.

Khouider, B., and A. J. Majda, 2006b: Multicloud convective parametrizations with crude vertical structure. *Theoretical and Computational Fluid Dynamics*, **20 (5-6)**, 351–375.

Khouider, B., and A. J. Majda, 2006c: A simple multicloud parameterization for convectively coupled tropical waves. part I: Linear analysis. *Journal of the atmospheric sciences*, **63 (4)**, 1308–1323.

Khouider, B., and A. J. Majda, 2007: A simple multicloud parameterization for convectively coupled tropical waves. part II: Nonlinear simulations. *Journal of the atmospheric sciences*, **64 (2)**, 381–400.

Khouider, B., and A. J. Majda, 2008a: Equatorial convectively coupled waves in a simple multicloud model. *Journal of the Atmospheric Sciences*, **65 (11)**, 3376–3397.

Khouider, B., and A. J. Majda, 2008b: Multicloud models for organized tropical convection: Enhanced congestus heating. *Journal of the Atmospheric Sciences*, **65 (3)**, 895–914.

Khouider, B., and M. W. Moncrieff, 2015: Organized convection parameterization for the ITCZ. *Journal of the Atmospheric Sciences*, **72 (8)**, 3073–3096.

Khouider, B., A. St-Cyr, A. J. Majda, and J. Tribbia, 2011: The MJO and convectively coupled waves in a coarse-resolution gcm with a simple multicloud parameterization. *Journal of the Atmospheric Sciences*, **68 (2)**, 240–264.

Kiladis, G. N., M. C. Wheeler, P. T. Haertel, K. H. Straub, and P. E. Roundy, 2009: Convectively coupled equatorial waves. *Reviews of Geophysics*, **47 (2)**.

Lindzen, R. S., and S. Nigam, 1987: On the role of sea surface temperature gradients in forcing low-level winds and convergence in the tropics. *Journal of the Atmospheric Sciences*, **44 (17)**, 2418–2436.

Majda, A. J., 2003: *Introduction to PDEs and Waves for the Atmosphere and Ocean*, Vol. 9. American Mathematical Soc.

Majda, A. J., 2007: New multiscale models and self-similarity in tropical convection. *Journal of the atmospheric sciences*, **64 (4)**, 1393–1404.

Majda, A. J., and R. Klein, 2003: Systematic multiscale models for the tropics. *Journal of the Atmospheric Sciences*, **60 (2)**, 393–408.

Majda, A. J., and M. G. Shefter, 2001: Models for stratiform instability and convectively coupled waves. *Journal of the atmospheric sciences*, **58 (12)**, 1567–1584.

Majda, A. J., and Q. Yang, 2016: A multiscale model for the intraseasonal impact of the diurnal cycle over the maritime continent on the Madden–Julian oscillation. *Journal of the Atmospheric Sciences*, **73 (2)**, 579–604.

Mapes, B. E., 2000: Convective inhibition, subgrid-scale triggering energy, and stratiform instability in a toy tropical wave model. *Journal of the Atmospheric Sciences*, **57 (10)**, 1515–1535.

Matsuno, T., 1966: Quasi-geostrophic motions in the equatorial area. *J. Meteor. Soc. Japan*, **44 (1)**, 25–43.

McFarlane, N., 1987: The effect of orographically excited gravity wave drag on the general circulation of the lower stratosphere and troposphere. *Journal of the atmospheric sciences*, **44 (14)**, 1775–1800.

Moncrieff, M., 1978: The dynamical structure of two-dimensional steady convection in constant vertical shear. *Quarterly Journal of the Royal Meteorological Society*, **104 (441)**, 543–567.

Moncrieff, M., 1981: A theory of organized steady convection and its transport properties. *Royal Meteorological Society, Quarterly Journal*, **107**, 29–50.

Moncrieff, M. W., 1992: Organized convective systems: Archetypal dynamical models, mass and momentum flux theory, and parametrization. *Quarterly Journal of the Royal Meteorological Society*, **118 (507)**, 819–850.

Moncrieff, M. W., C. Liu, and P. Bogenschutz, 2017: Simulation, modeling, and dynamically based parameterization of organized tropical convection for global climate models. *Journal of the Atmospheric Sciences*, **74 (5)**, 1363–1380.

Nakazawa, T., 1988: Tropical super clusters within intraseasonal variations over the western pacific. *J. Meteor. Soc. Japan*, **66 (6)**, 823–839.

Neelin, J. D., and N. Zeng, 2000: A quasi-equilibrium tropical circulation model-formulation. *Journal of the atmospheric sciences*, **57 (11)**.

Straub, K. H., and G. N. Kiladis, 2002: Observations of a convectively coupled Kelvin wave in the eastern pacific ITCZ. *Journal of the atmospheric sciences*, **59 (1)**, 30–53.

Straub, K. H., G. N. Kiladis, and P. E. Ciesielski, 2006: The role of equatorial waves in the onset of the south china sea summer monsoon and the demise of El Niño during 1998. *Dynamics of atmospheres and oceans*, **42 (1)**, 216–238.

Tao, W.-K., and M. W. Moncrieff, 2009: Multiscale cloud system modeling. *Reviews of Geophysics*, **47 (4)**.

Toma, V. E., and P. J. Webster, 2010a: Oscillations of the intertropical convergence zone and the genesis of easterly waves. part I: diagnostics and theory. *Climate dynamics*, **34 (4)**, 587–604.

Toma, V. E., and P. J. Webster, 2010b: Oscillations of the intertropical convergence zone and the genesis of easterly waves part II: numerical verification. *Climate dynamics*, **34 (4)**, 605–613.

Tulich, S. N., and B. E. Mapes, 2008: Multiscale convective wave disturbances in the tropics: Insights from a two-dimensional cloud-resolving model. *Journal of the Atmospheric Sciences*, **65 (1)**, 140–155.

Wallace, J., and L. Chang, 1972: On the application of satellite data on cloud brightness to the study of tropical wave disturbances. *Journal of the Atmospheric Sciences*, **29 (7)**, 1400–1403.

Wang, B., and T. Li, 1993: A simple tropical atmosphere model of relevance to short-term climate variations. *Journal of the atmospheric sciences*, **50 (2)**, 260–284.

Wang, H., and R. Fu, 2007: The influence of amazon rainfall on the atlantic ITCZ through convectively coupled Kelvin waves. *Journal of climate*, **20 (7)**, 1188–1201.

Yang, G.-Y., B. Hoskins, and J. Slingo, 2007a: Convectively coupled equatorial waves. part I: Horizontal and vertical structures. *Journal of the Atmospheric Sciences*, **64 (10)**, 3406–3423.

Yang, G.-Y., B. Hoskins, and J. Slingo, 2007b: Convectively coupled equatorial waves. part II: Propagation characteristics. *Journal of the Atmospheric Sciences*, **64 (10)**, 3424–3437.

Yang, G.-Y., B. Hoskins, and J. Slingo, 2007c: Convectively coupled equatorial waves. part III: Synthesis structures and their forcing and evolution. *Journal of the Atmospheric Sciences*, **64 (10)**, 3438–3451.

Yang, Q., and A. J. Majda, 2014: A multi-scale model for the intraseasonal impact of the diurnal cycle of tropical convection. *Theoretical and Computational Fluid Dynamics*, **28 (6)**, 605–633.

Yang, Q., and A. J. Majda, 2017: Upscale impact of mesoscale disturbances of tropical convection on synoptic-scale equatorial waves in two-dimensional flows. *submitted to Journal of the Atmospheric Sciences*.

Zangvil, A., 1975: Temporal and spatial behavior of large-scale disturbances in tropical cloudiness deduced from satellite brightness data. *Monthly Weather Review*, **103 (10)**, 904–920.

LIST OF TABLES

TABLE 1. Physical parameters and dimensional scaling in the MESD model.

	Physical variables	Symbolic notation	Value
Constant	Buoyancy frequency	N	$10^{-2}s^{-1}$
	Height	H	$15.7km$
	Dry kelvin wave speed	c	$50ms^{-1}$
	Rossby parameter	β	$2.23\times10^{-11}s^{-1}m^{-1}$
Synoptic scale	Horizontal spatial scale	X,Y	$1500km$
	Temporal scale	t	$8.3hrs$
	Horizontal velocity	U,V	$5ms^{-1}$
	Vertical velocity	W	$1.6\times10^{-2}ms^{-1}$
	Pressure perturbation	P	$250m^2s^{-2}$
	Potential temperature anomalies	Θ	$3.3K$
	Horizontal momentum forcing	S_u,S_v	$15ms^{-1}day^{-1}$
	Thermal forcing	S_θ	$10Kday^{-1}$
Mesoscale	Horizontal spatial scale	x,y	$150km$
	Temporal scale	τ	$50min$
	Horizontal velocity	u,v	$5ms^{-1}$
	Vertical velocity	w	$1.6\times10^{-1}ms^{-1}$
	Pressure perturbation	p	$250m^2s^{-2}$
	Potential temperature anomalies	θ	$3.3K$
	Horizontal momentum forcing	s_u,s_v	$150ms^{-1}day^{-1}$
	Thermal forcing	s_θ	$100Kday^{-1}$

LIST OF FIGURES

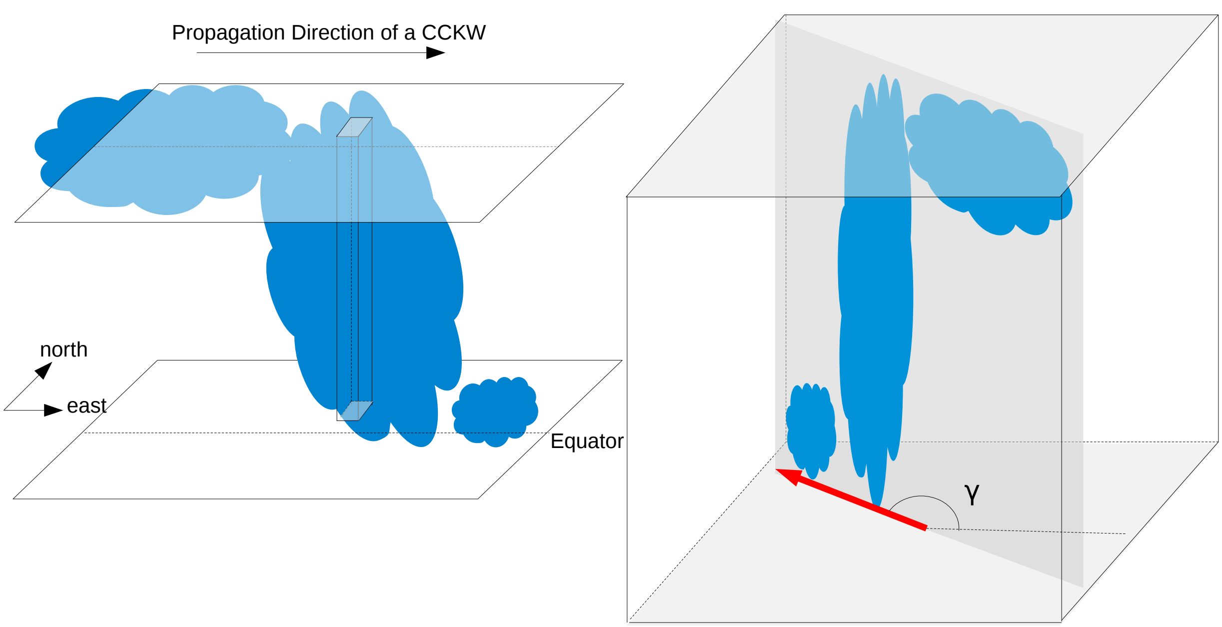

868 FIG. 1. Conceptual diagram for a CCKW with embedded mesoscale disturbances. The left diagram shows
869 an eastward-moving CCKW (blue) on the synoptic scale, where the rectangular cuboid denotes a mesoscale
870 domain. The right diagram (zoom in the rectangular cuboid in the left diagram) shows a MCS propagating at a
871 tilt angle γ in the mesoscale domain.

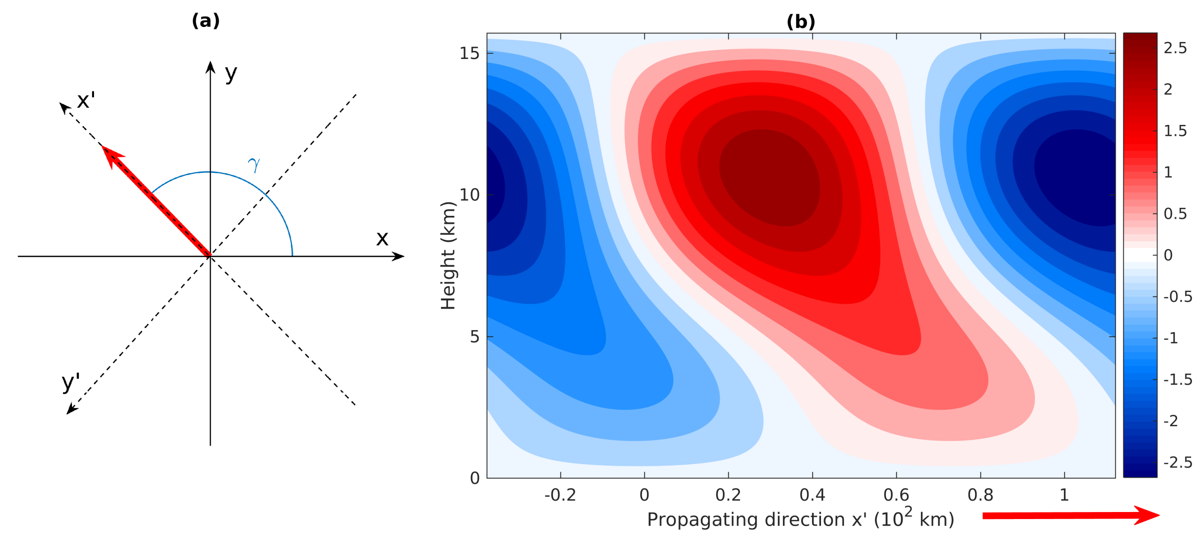

FIG. 2. Vertical profile of mesoscale heating in the new reference frame. In panel (a), the normal reference frame is denoted by x-axis (east) and y-axis (north) in solid lines. The new reference frame with x'-axis and y'-axis in dashed lines is derived by anticlockwise rotating the normal reference frame by an angle γ. The red bold arrow shows the propagation direction of mesoscale heating. Panel (b) shows the vertical profile of mesoscale heating in the new reference frame. The dimensional unit is 100 $Kday^{-1}$.

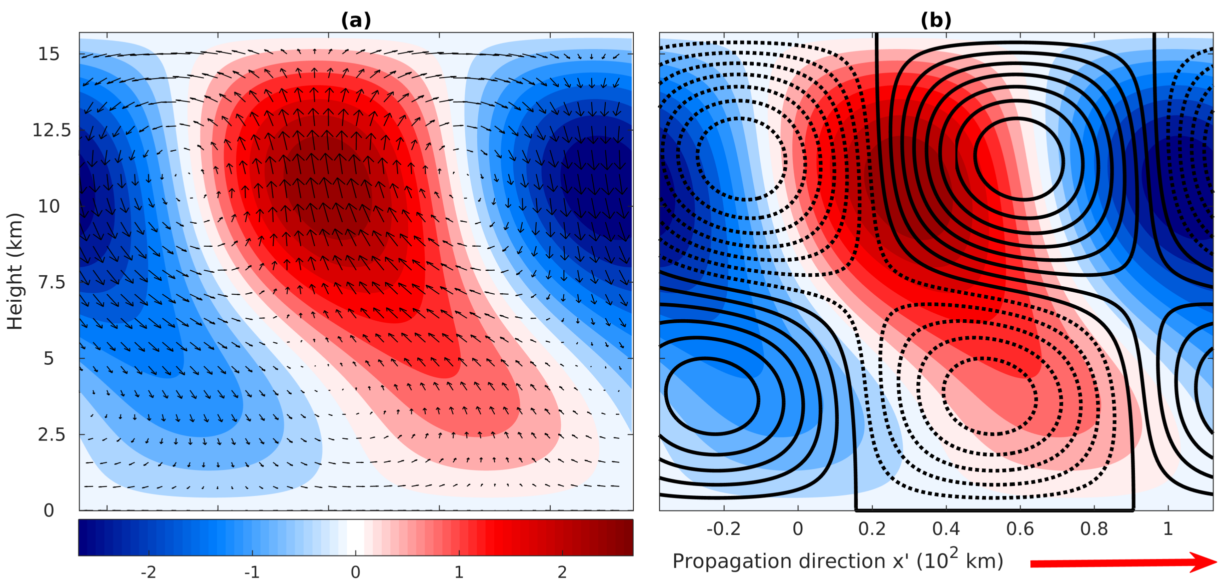

FIG. 3. Vertical profiles of zonal velocity, vertical velocity and potential temperature anomalies along the propagation direction of mesoscale heating. The arrows in panel (a) show zonal and vertical velocity and the contours in panel (b) show potential temperature anomalies. The color in both panels shows mesoscale heating. The maximum magnitudes of zonal and vertical velocity are 3.72 ms^{-1} and 0.47 ms^{-1}, respectively. The contour interval of potential temperature anomalies is 0.1 K. The dimensional unit of mesoscale heating is 100 $Kday^{-1}$.

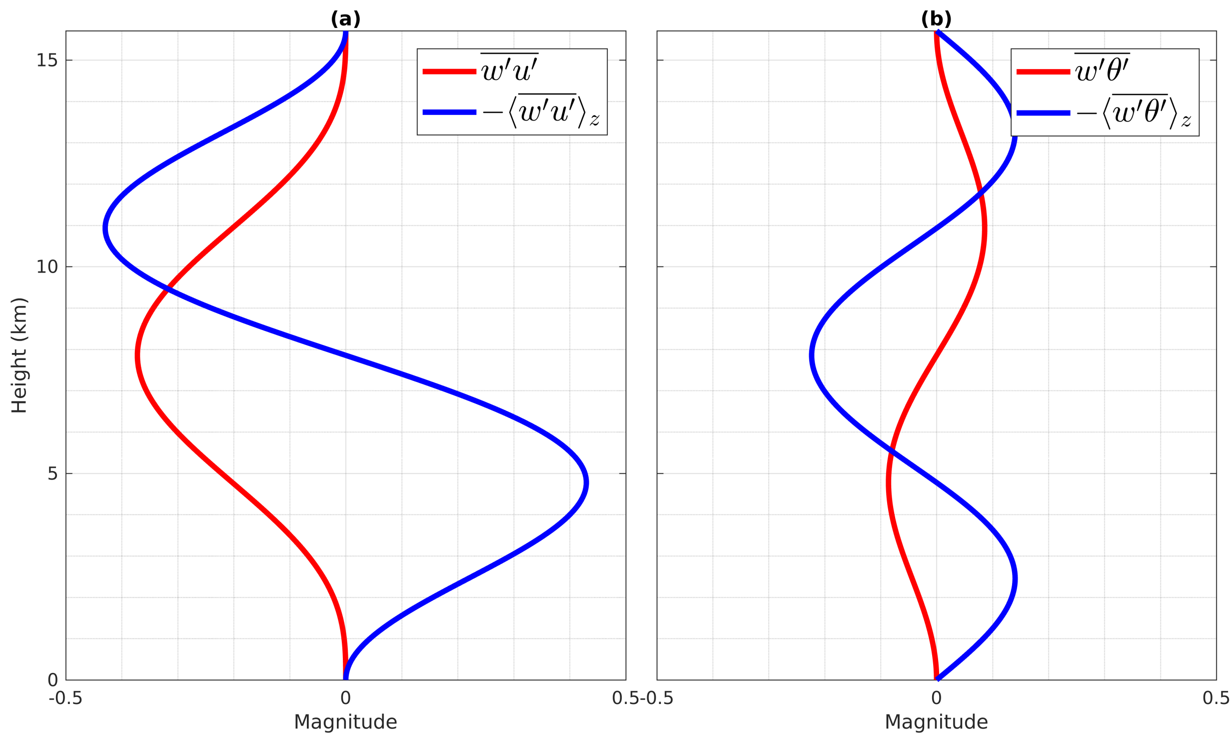

FIG. 4. Vertical profiles of eddy zonal momentum transfer and eddy heat transfer. Panel (a) shows eddy zonal momentum transfer (blue) and the associated eddy flux (red). Panel (b) shows eddy heat transfer (blue) and the associated eddy flux (red). One dimensionless unit of eddy zonal momentum and eddy heat transfer is 15 $ms^{-1}day^{-1}$ and 10 $Kday^{-1}$, respectively.

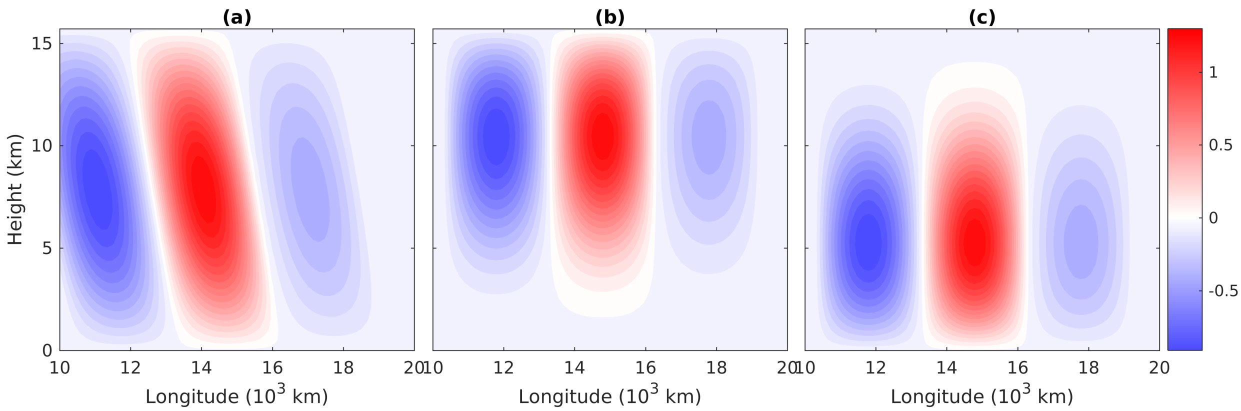

886 FIG. 5. Vertical profile of mean heating at the equator. The panel from left to right show (a) tilted mean heating, (b) top-heavy upright mean heating, (c) bottom-heavy upright mean heating. The dimensional unit of mean heating is 10 $Kday^{-1}$.

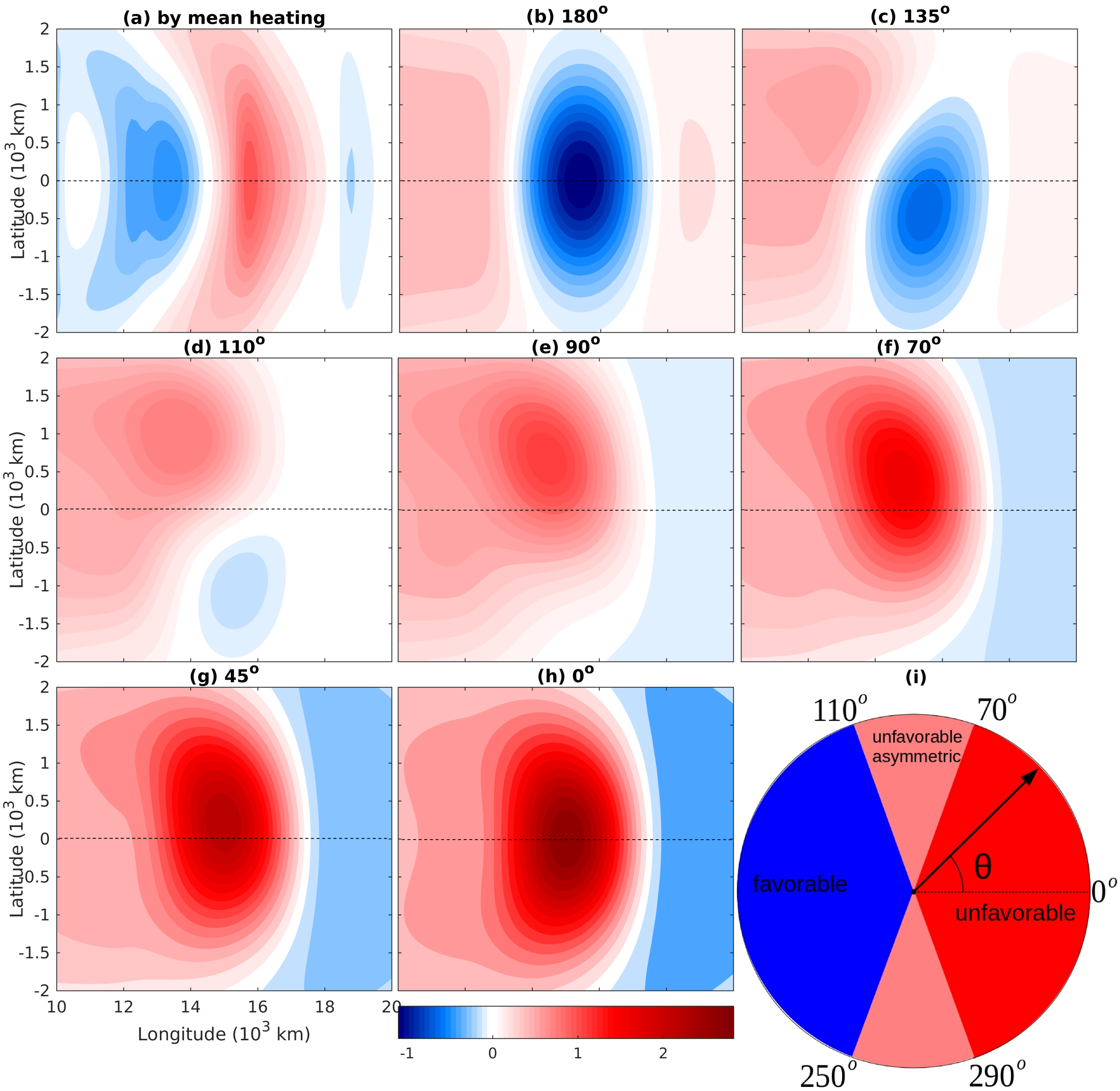

FIG. 6. Horizontal profile of potential temperature anomalies at the lower troposphere (2.62 km) in the longitude-latitude diagram. Panel (a) shows potential temperature anomalies induced by tilted mean heating. Panels (b-h) shows those induced by eddy terms at tilt angles 180°, 135°, 110°, 90°, 70°, 45°, 0°. Panel (i) shows favorability of convection in different tilt angle cases (blue: favorable; pink: unfavorable, asymmetric; red: unfavorable). The dimensional unit of potential temperature anomalies is K.

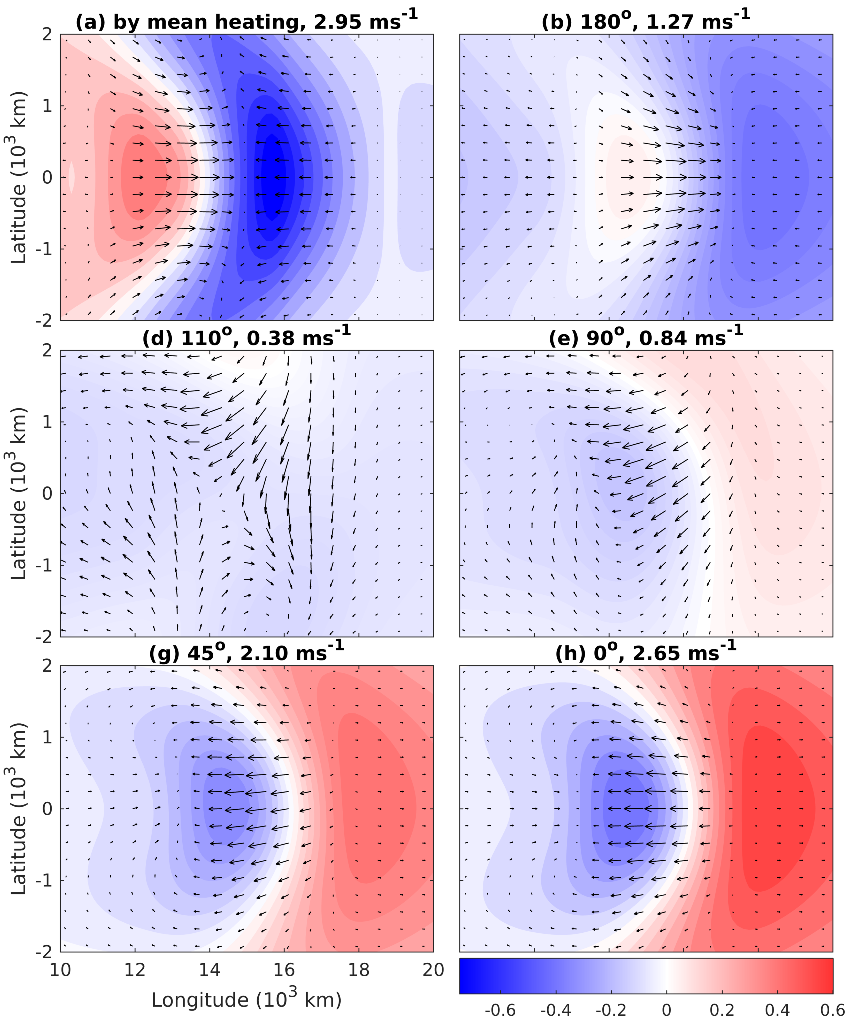

FIG. 7. Horizontal profiles of horizontal velocity (arrow) and pressure perturbation (color) at the surface in the longitude-latitude diagram. Panel (a) shows flow field induced by mean heating. Panels (b-h) show that induced by eddy terms at tilt angles 180°, 135°, 110°, 90°, 70°, 45°, 0°. The dimensional units of horizontal velocity and pressure perturbation are ms^{-1} and 100 m^2s^{-2} per mass. The maximum magnitude of horizontal velocity is shown in the title of each panel.

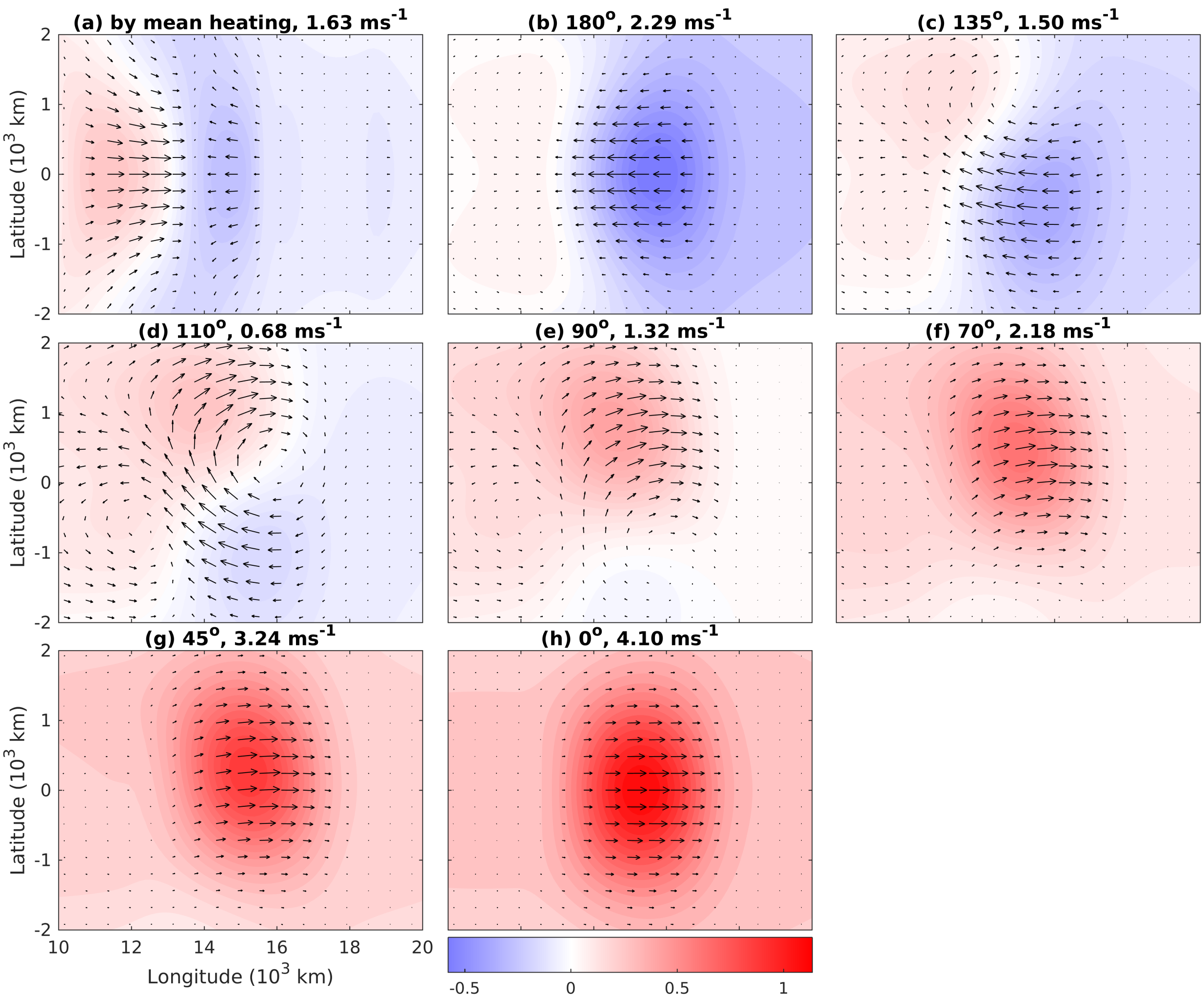

FIG. 8. The same as Fig.7 but at the lower troposphere (5.24 km).

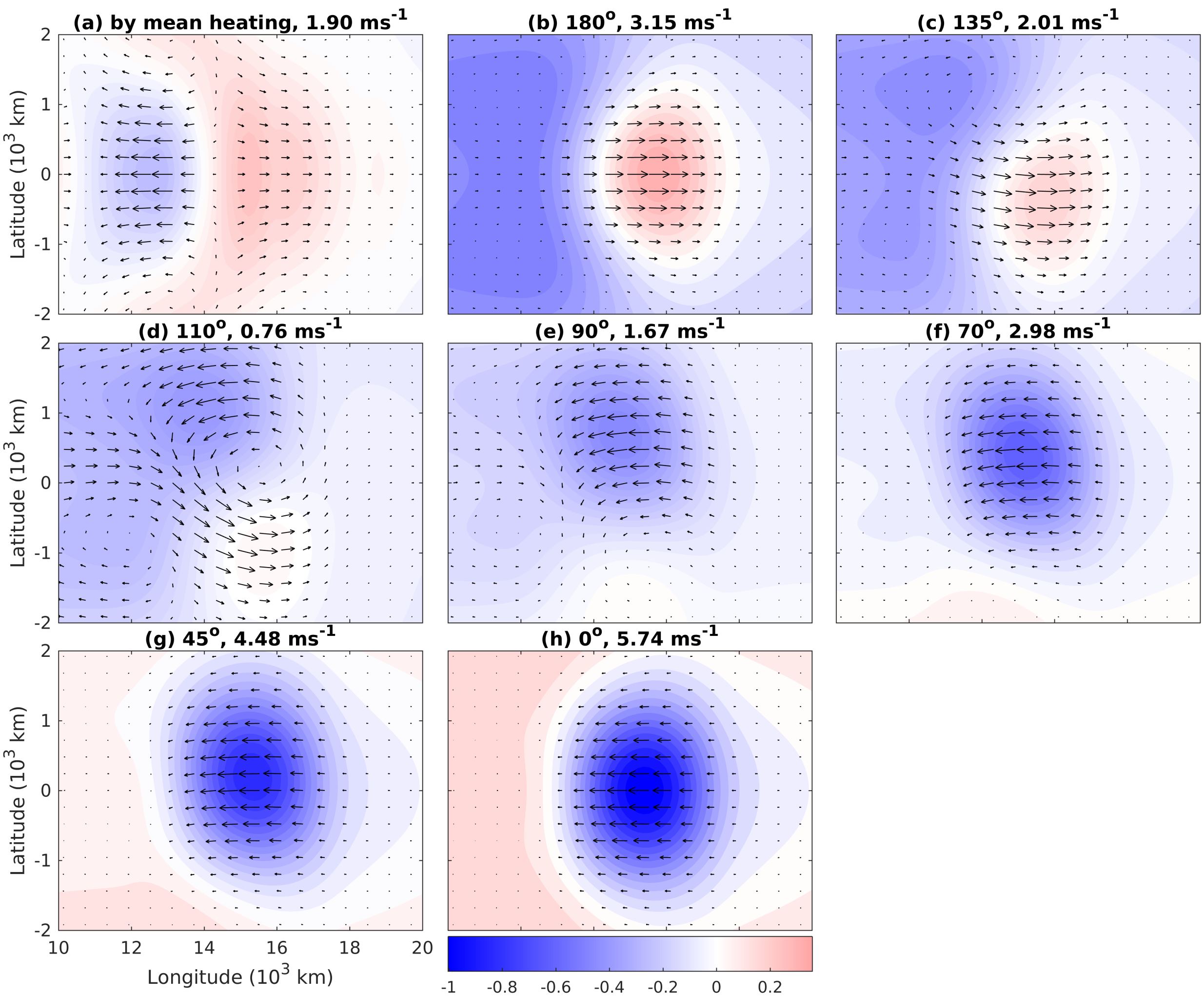

FIG. 9. The same as Fig.7 but at the upper troposphere (10.47 km).

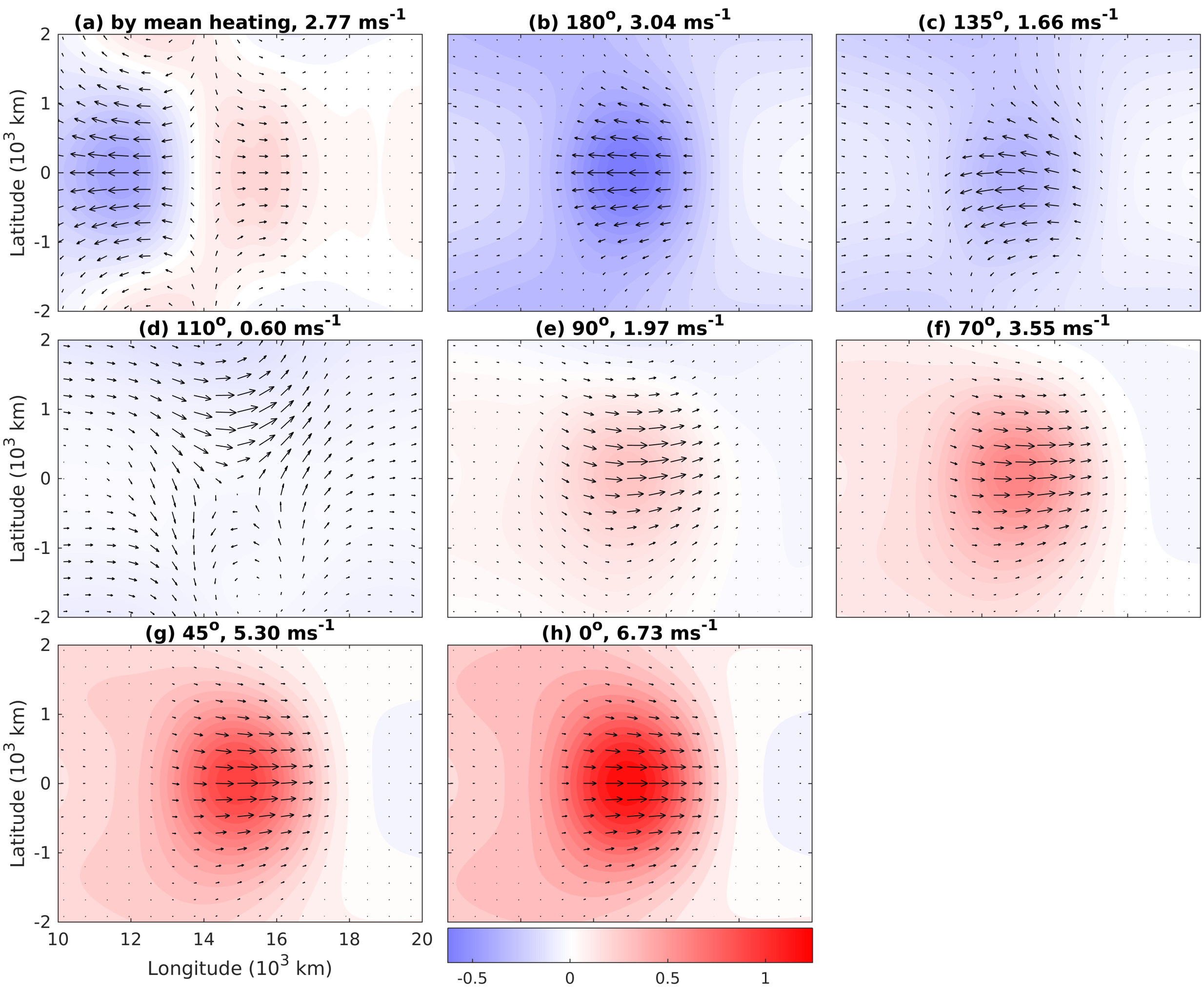

FIG. 10. The same as Fig.7 but at the top of the troposphere (15.70 km).

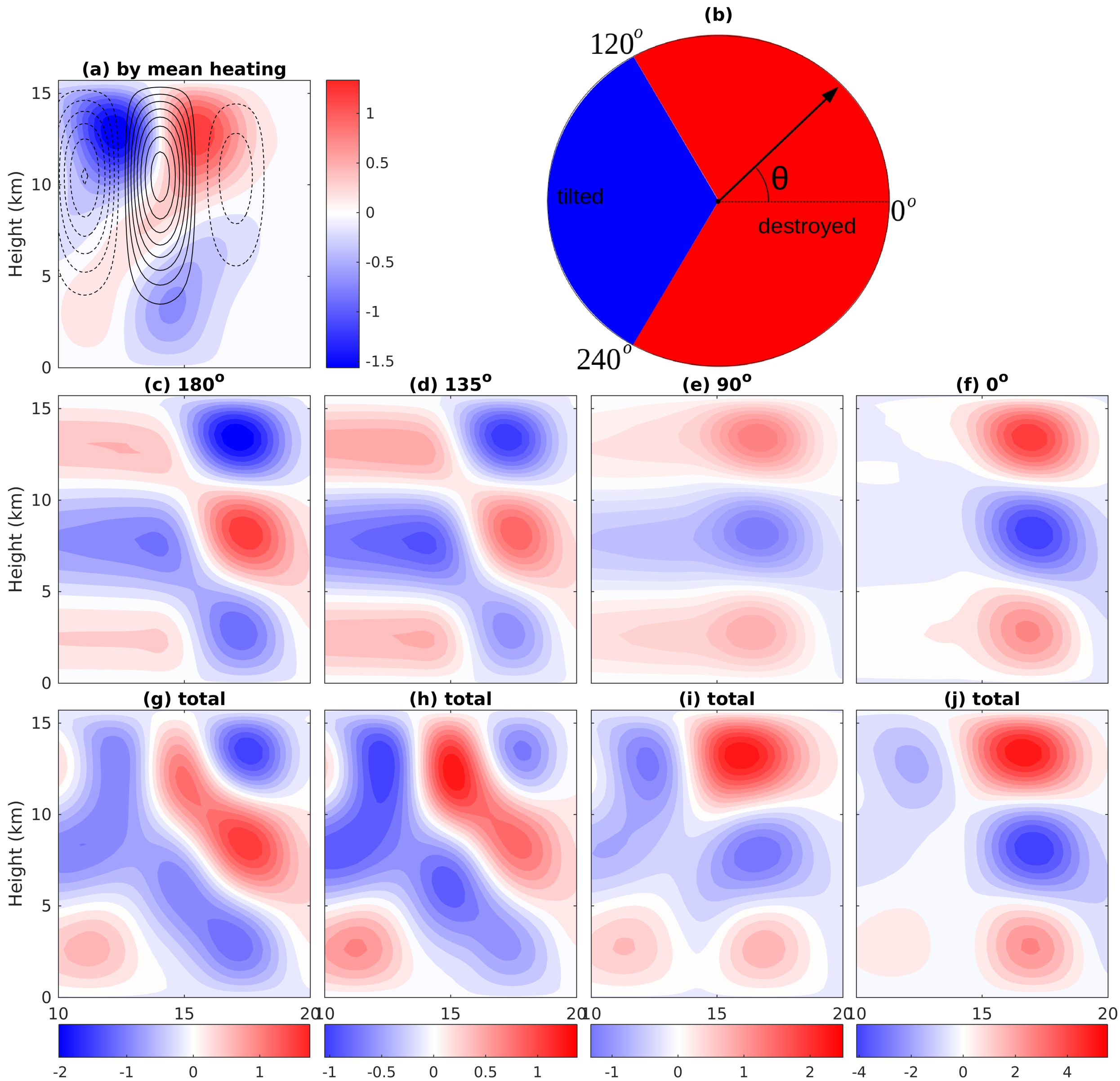

FIG. 11. Vertical profile of potential temperature anomalies at the equator in the longitude-height diagram. Panel (a) shows potential temperature anomalies induced by top-heavy upright mean heating. Panels (c-f) show those induced by eddy terms at tilt angles 180°, 135°, 90°, 0°. Panels (g-j) show total anomalies induced by both mean heating and eddy terms at the same tilt angle as the panel above it. Panel (b) shows the upscale impact of mesoscale fluctuations at different tilt angles on the tilted vertical structure (blue: tilted; red: destroyed). The contours in panel (a) show mean heating. The dimensional unit of potential temperature anomalies is K.

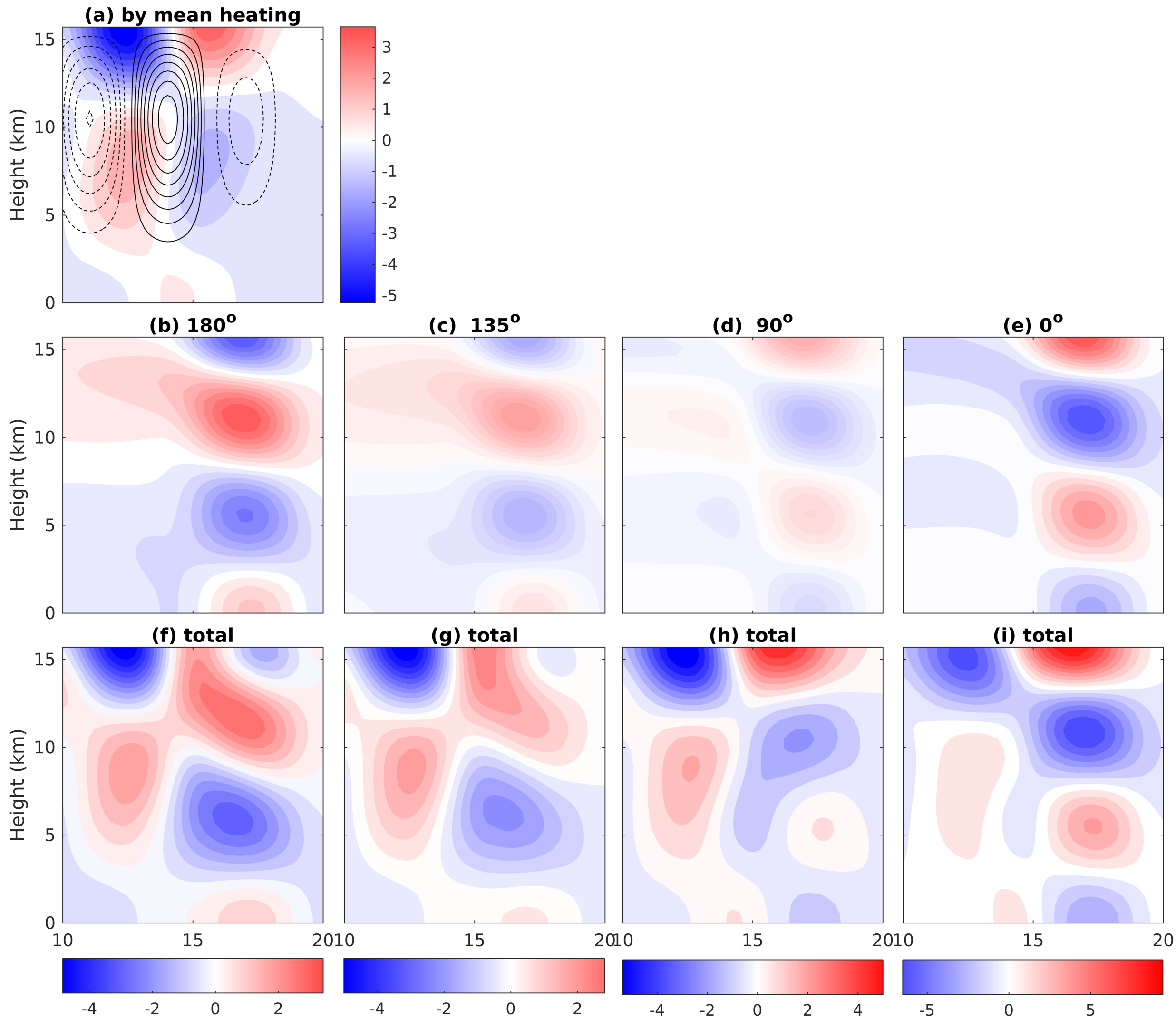

FIG. 12. Vertical profile of zonal velocity at the equator in the longitude-height diagram. Panel (a) shows zonal velocity induced by top-heavy upright mean heating. Panels (c-f) show that induced by eddy terms at tilt angles 180°, 135°, 90°, 0°. Panels (g-j) show total zonal velocity induced by both mean heating and eddy terms at the same tilt angle as the panel above it. The contours in panel (a) show mean heating. The dimensional unit of zonal velocity is ms^{-1}.

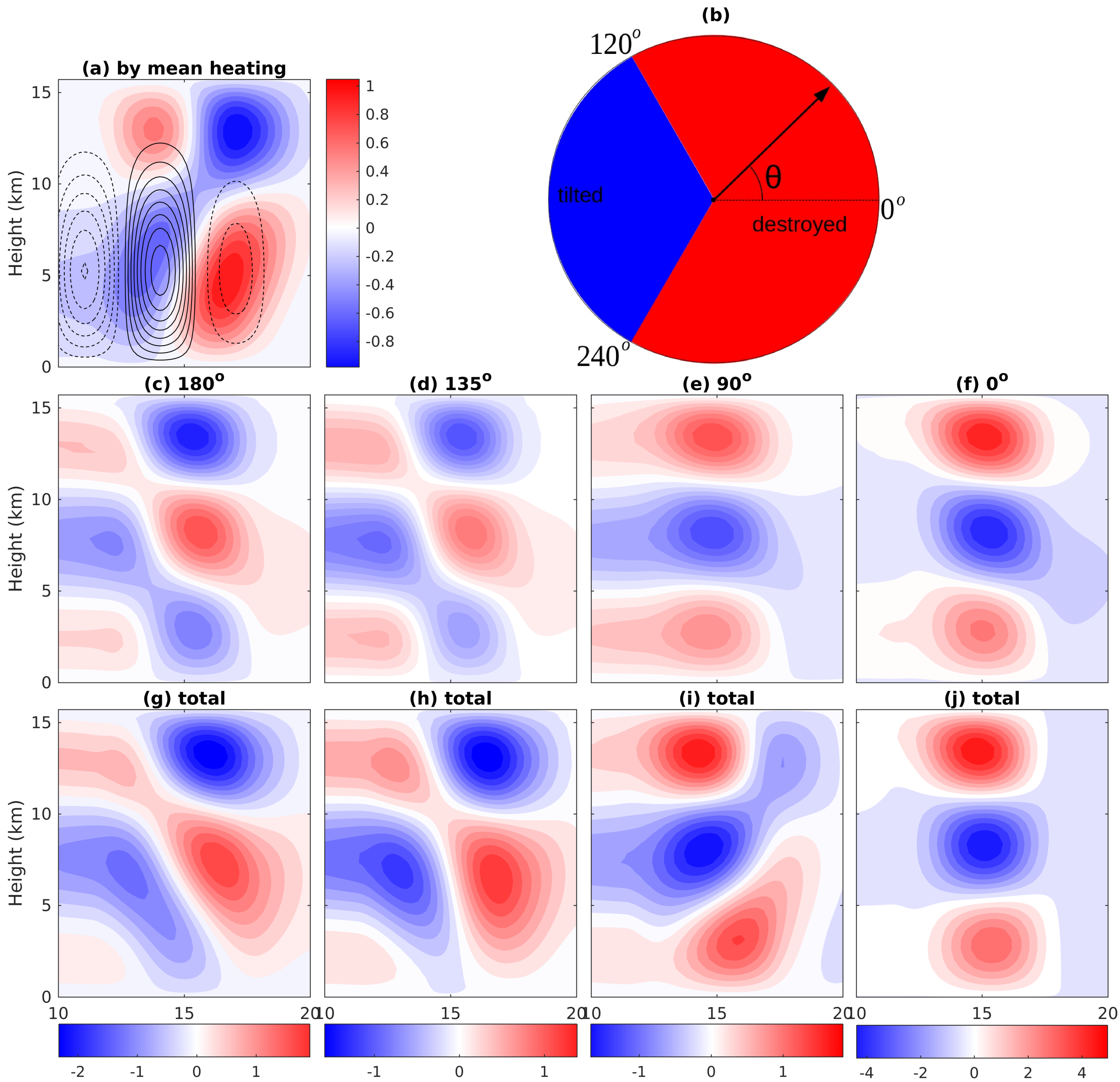

FIG. 13. The same as Fig.11 but for bottom-heavy upright mean heating case.

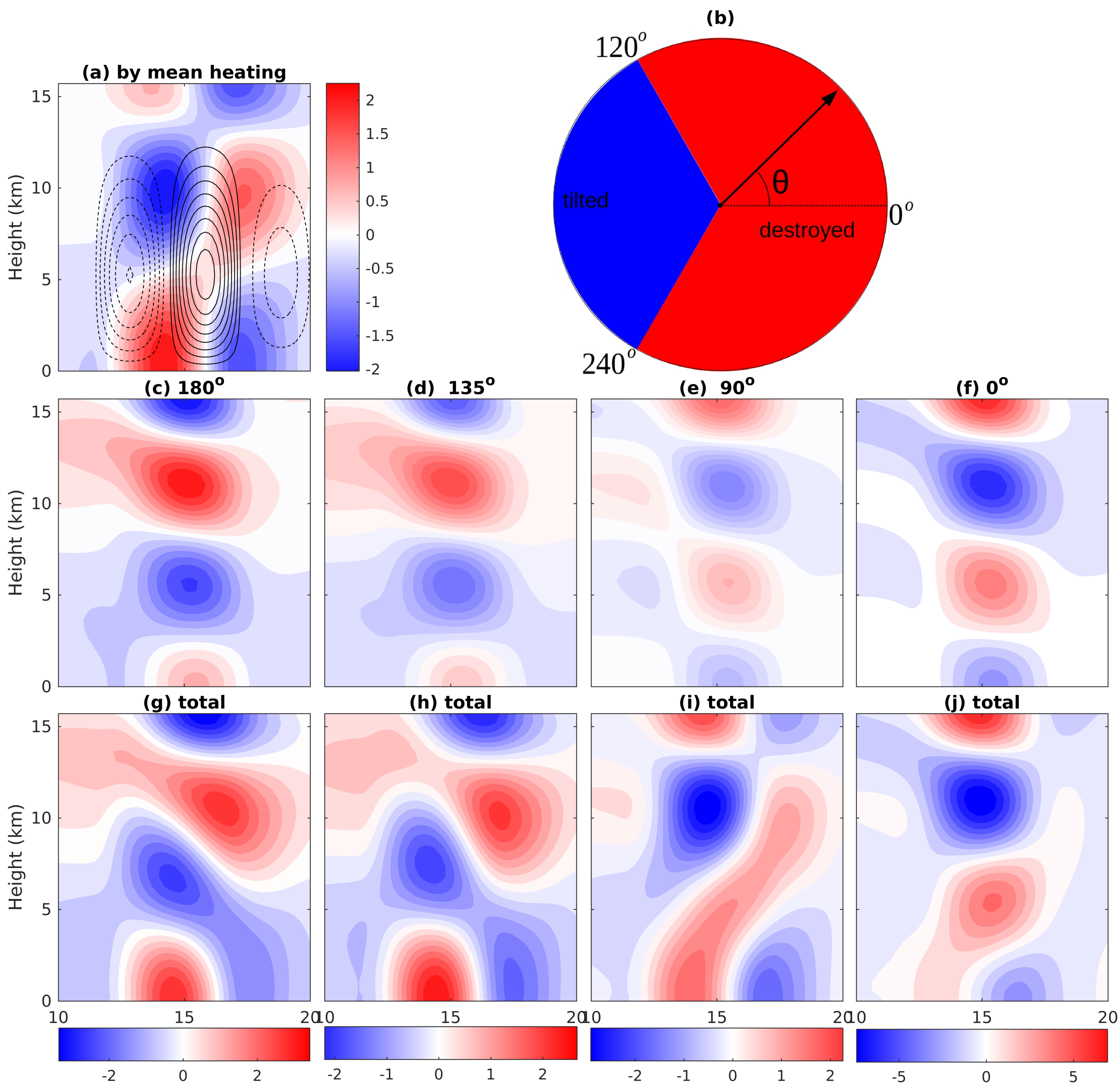

FIG. 14. The same as Fig.12 but for bottom-heavy upright mean heating case.

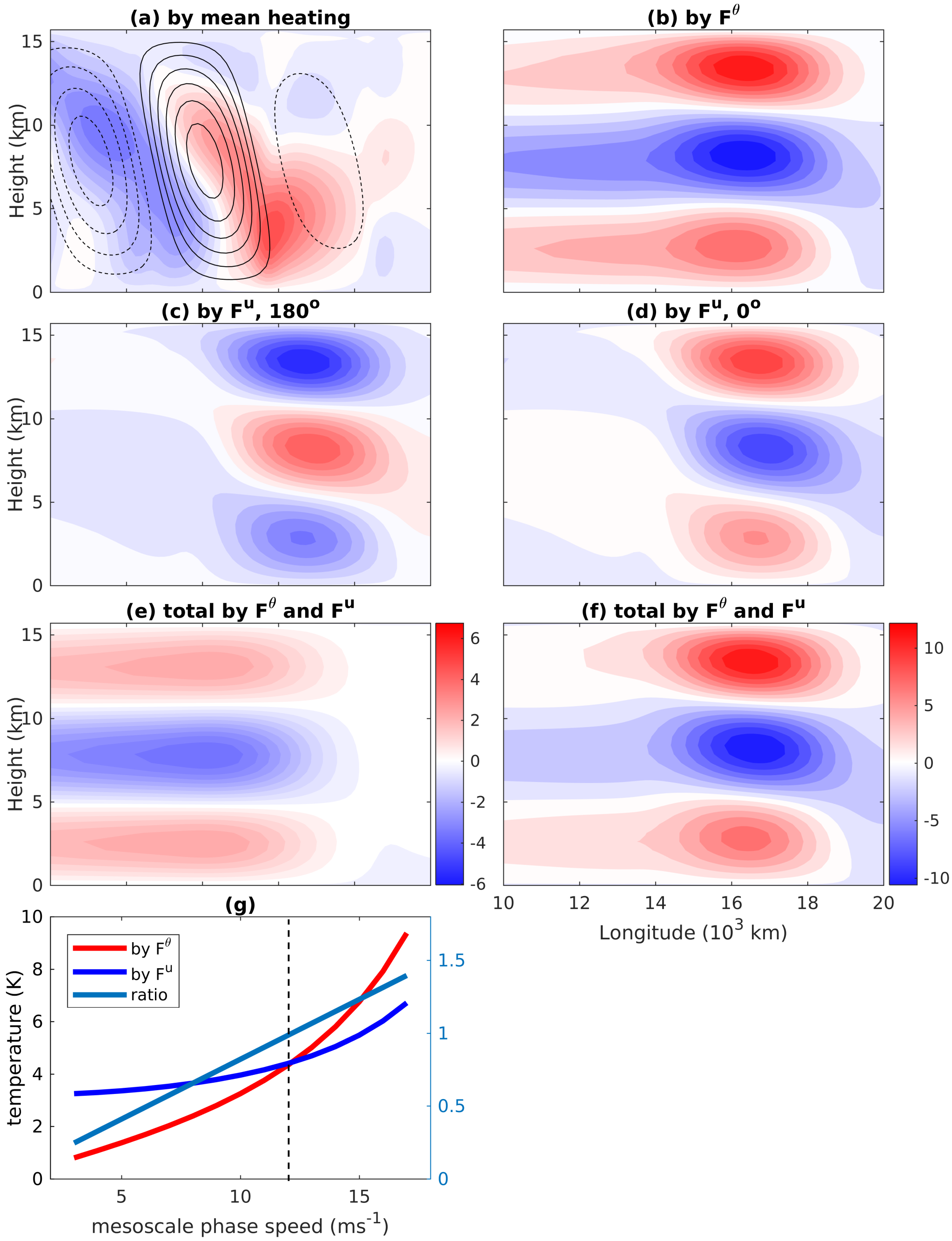

FIG. 15. Vertical profile of potential temperature anomalies at the equator in the fast propagating mesoscale heating case (15 ms^{-1}) in the longitude-height diagram. Panel (a) shows potential temperature anomalies induced by tilted mean heating. Panel (b) shows those induced by eddy heat transfer. Panels (c-d) show those induced by eddy momentum transfer at the tilt angle (c) 180°, (d) 0°. Panels (e-f) show total anomalies induced by eddy terms at the tilt angle (e) 180°, (f) 0°. Panel (g) shows maximum magnitude of potential temperature anomalies induced by eddy terms at different propagation speeds of mesoscale heating. The contours in panel (a) shows tilted mean heating (contour interval is 1.5 $K day^{-1}$). The dimensional unit of potential temperature anomalies is K.

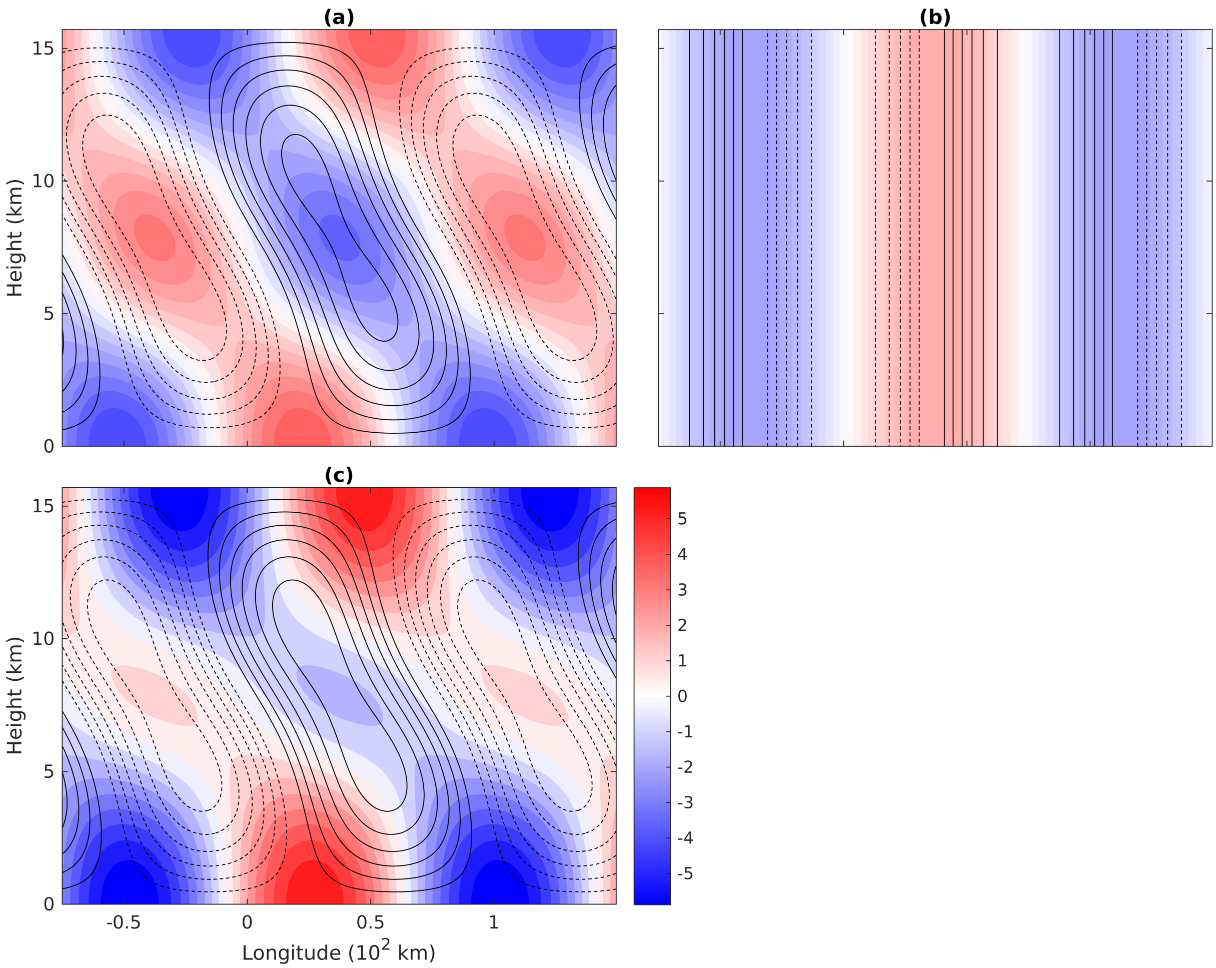

FIG. 16. Vertical profile of zonal velocity in the longitude-height diagram. In panel (a), the color shows zonal velocity induced by mesoscale heating and the contours show mesoscale heating (contour interval 65 $Kday^{-1}$). In panel (b), the color shows zonal velocity induced by mesoscale barotropic momentum forcing, and the contours show mesoscale barotropic momentum forcing (contour interval 22.5 $ms^{-1}day^{-1}$). In panel (c), the color shows total zonal velocity and the contours show vertical velocity (contour interval 0.1 ms^{-1}). The dimensional unit of zonal velocity is ms^{-1}.

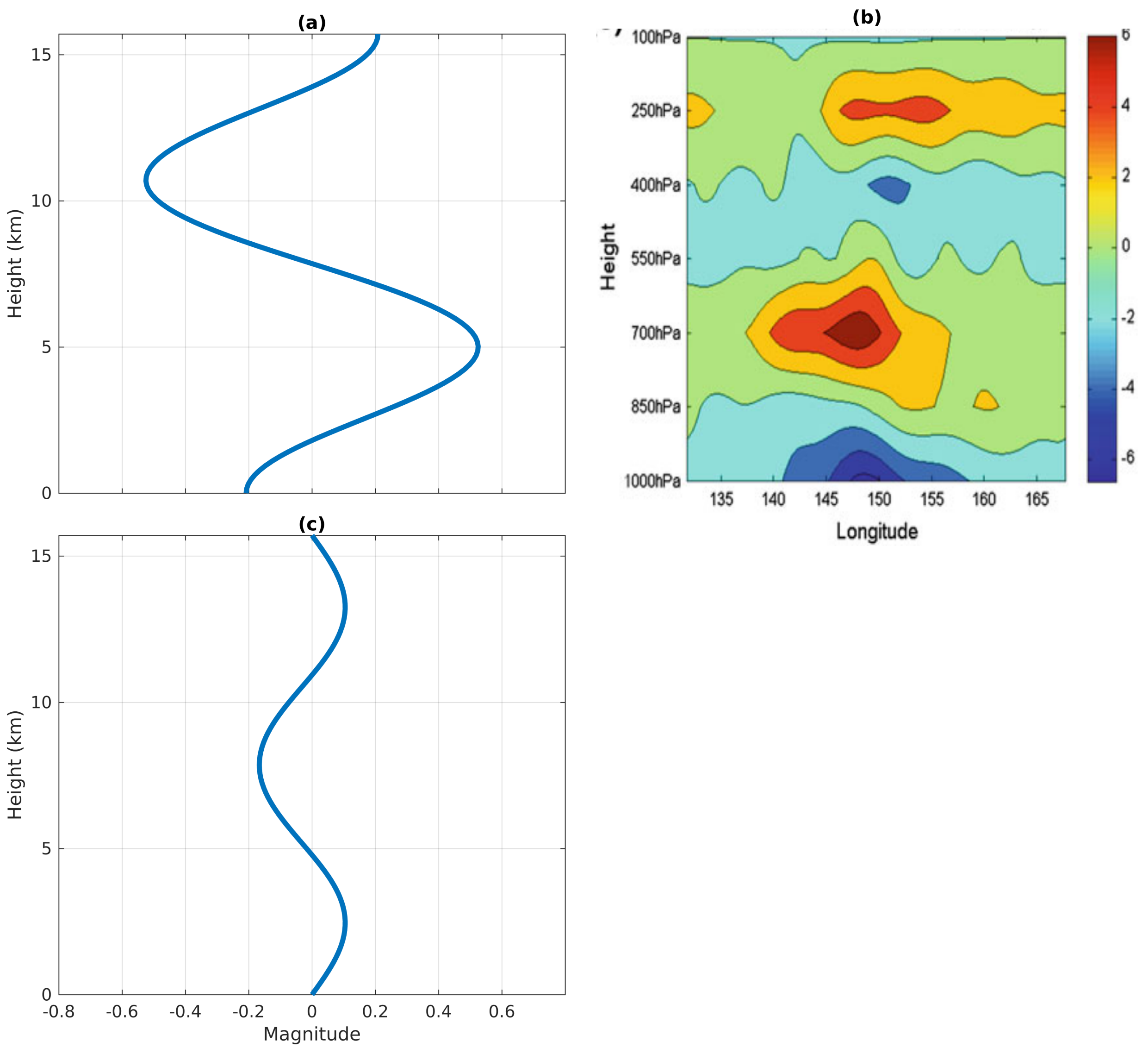

924 FIG. 17. Vertical profile of eddy zonal momentum transfer and eddy heat transfer induced by slowly eastward-propagating mesoscale heating and mesoscale barotropic momentum forcing. Panel (a) shows eddy zonal momentum transfer. Panel (b) is adjusted from Figure 11c of Khouider and Han (2013). Panel (c) shows eddy heat transfer. The dimensional units of eddy zonal momentum transfer and eddy heat transfer are 15 $ms^{-1}day^{-1}$ and 10 $Kday^{-1}$, respectively.

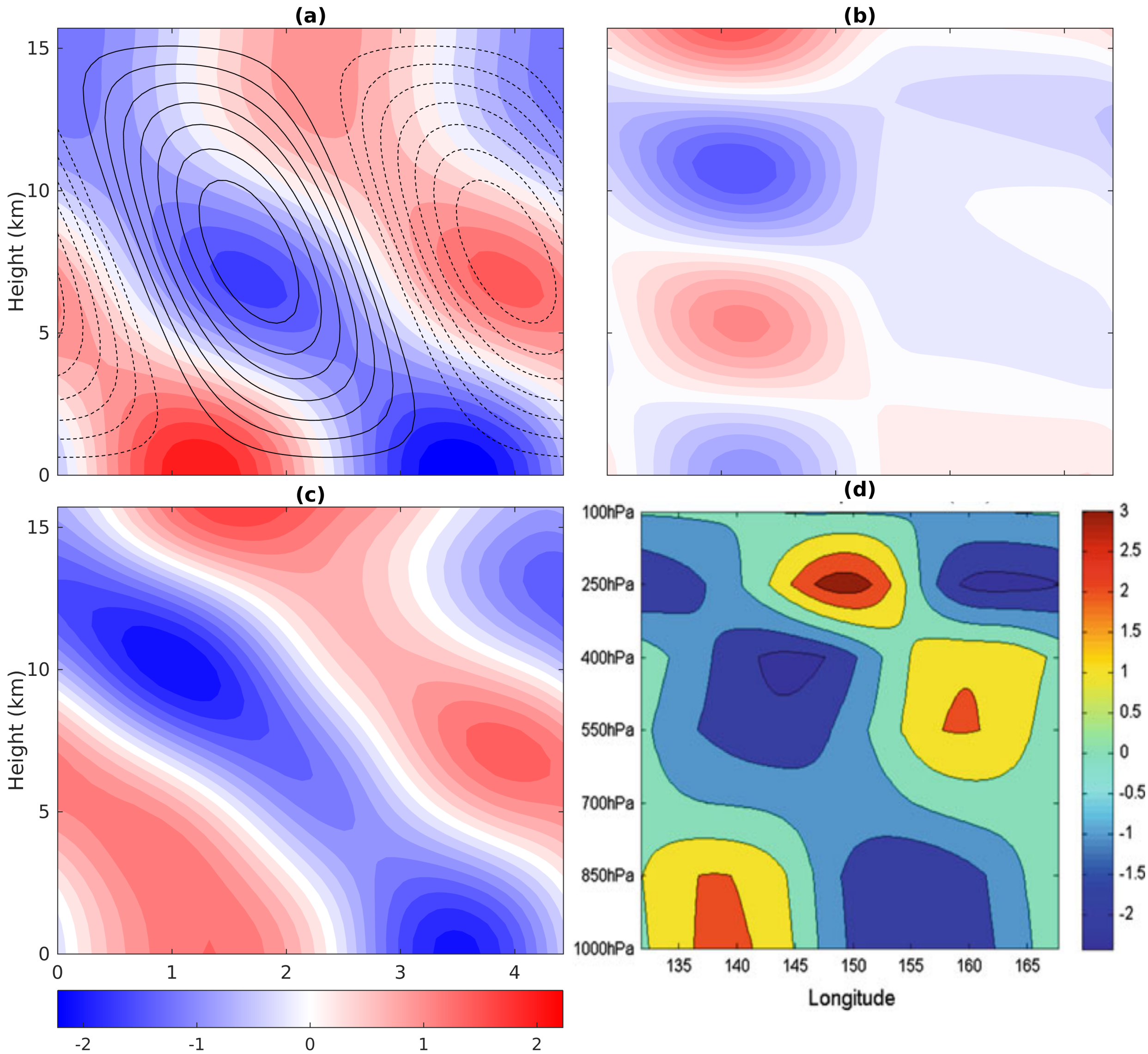

FIG. 18. Vertical profile of zonal velocity at the equator. In panel (a), the color shows zonal velocity induced by mean heating and the contours show mean heating (contour interval is 1.25 $Kday^{-1}$). Panels (b) shows that induced by eddy terms, and panel (c) shows total zonal velocity. Panel (d) is adjusted from Figure 11d of Khouider and Han (2013). The dimensional unit of zonal velocity is ms^{-1}.

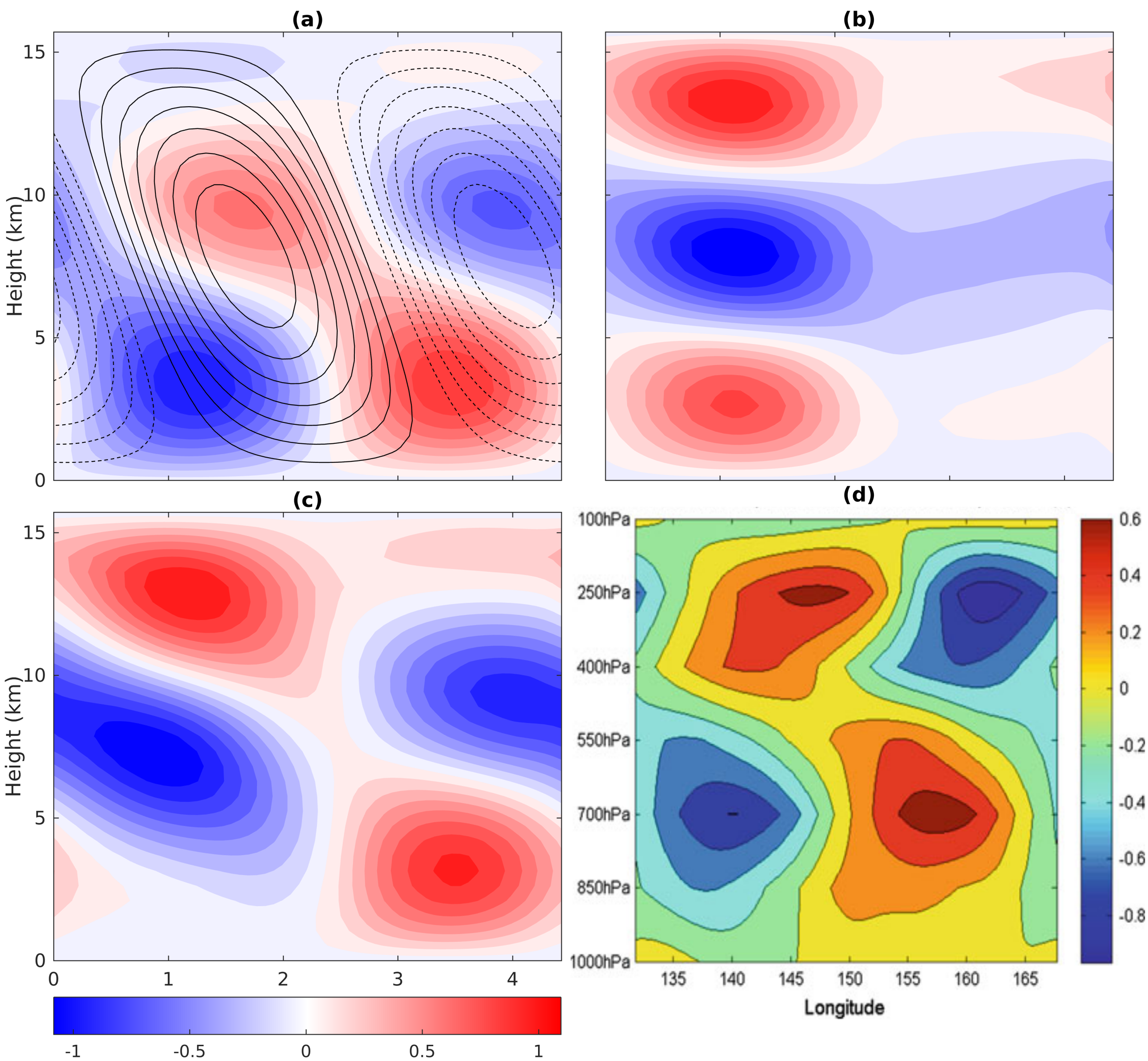

FIG. 19. Vertical profile of potential temperature anomalies at the equator. In panel (a), the color shows potential temperature anomalies induced by mean heating, and the contours show mean heating (contour interval is 1.25 $Kday^{-1}$). Panel (b) shows those induced by eddy terms, and panel (c) shows total anomalies. Panel (d) is adjusted from Figure 9d of Khouider and Han (2013). The dimensional unit of potential temperature anomalies is K.